공학석사 학위논문

Estimation of Punching Shear on UHPC Slab

UHPC 슬래브의 뚫림전단 연구

2015 년 2 월

서울대학교 대학원

건축학과

박 지 현

Estimation of Punching Shear on UHPC Slab

지도 교수 홍 성 걸

이 논문을 공학석사 학위논문으로 제출함
2014 년 11월

서울대학교 대학원
건축학과
박 지 현

박지현의 공학석사 학위논문을 인준함
2015 년 2 월

위 원 장 _____ (인)

부위원장 _____ (인)

위 원 _____ (인)

Abstract

Estimation of Punching Shear on UHPC Slab

Park, Ji-Hyun
Department of Architecture and Architectural Engineering
College of Engineering
Seoul National University

Nowadays, UHPC (High Performance Fiber Reinforced Concrete) is used widely with its remarkable performance, such as strength, ductility and durability. Due to the fibers in the UHPC which can control the tensile crack, the punching shear capacity of UHPC is higher than that of the conventional concrete, but the structural behavior of UHPC has not been determined completely. In this study, the data were analyzed for confirming the feasibility of the existing equations. In the preliminary study, the punching shear data of fiber-reinforced concrete slabs were analyzed for understanding the fiber effect. By analyzing experimental data, the equation that calculates the concrete, reinforcement and the fiber separately shows more accurate results. However, the method has problem that the coefficients for each terms are usually determined by experimental results. Therefore the relationship between the deformation based on material properties and the punching shear strength should be examined. In this paper, seven slabs with different thickness and fiber volume ratio were tested. In direct tension test, the crack width does not show the relationship according to the fiber volume ratio, but the tensile strength was increasing as the fiber volume ratio was increasing up to 1%. For the fiber content, 1% and 1.5% UHPC do not have big differences in tension test and punching shear test. However, the ratio of tensile strength and the punching shear strength was not proportional. The design tensile strength seems more proportional to the punching shear

strength. It is assumed for the reason of un-proportional relationship between the direct tensile strength and punching shear strength that the un-unified crack width and the fibers directivity difficult to control. The thicker slab thickness causes the increment of the punching shear strength with decrement of deformation capacity. The UHPC flat plate shows the wider punching shear area than the conventional concrete. The gentler strut angle for UHPC slab can be assumed in further study for UHPC failure mode. The punching shear strength equations tend to overestimate the thin slabs. From observing the deformation curve and the failure section, it is insisted that the thin slabs have flexural failure behavior. Due to the flexural behavior of the thin slabs, it could not resist the punching load as much as predicted. The minimum slab thickness should be proposed thicker than 40mm. By analyzing the test data, the JSCE code shows the least standard deviation, but it overestimates the punching shear strength. K-UHPC code results are close to the experimental value. However, the study for finding the relationship between the stress and the material property should be performed with effort to reduce the variance.

Keywords : Failure behavior; Punching shear strength; UHPC

Student Number : 2013-20560

Contents

List of Tables

List of Figures

Chapter 1. Introduction

1.1 General

Ultra-high performance concrete (UHPC) was developed to complement the concrete that has the brittle failure with increasing compressive strength. Unlike the original concrete, UHPC has high strength from 60MPa to 150MPa with good ductility and the durability. In this paper, the 120MPa UHPC was used for testing. UHPC has another merit that it can resist to the tensile strength due to the fiber content. The fiber acts like reinforcement bar in micro-structure system. The fiber controls the micro-crack by holding the matrix at the cracked section. The main characteristics of the composition of UHPC are lack of coarse aggregate and the reinforcement of steel fibers.

Only fine sand is contained in UHPC for the aggregate, and the low volume of water is used. High proportion of cementitious materials and low volume of water minimize the space between the particles. The fine aggregate is filled in the remainder of space. This causes the high density of UHPC, which means the increment in strength. UHPC is reinforced by long and thin steel fibers. The main advantage of containing steel fibers is post-cracking tensile response. The steel fibers prevent the micro-crack by bonding the cement matrix of cracked section.

The tensile strength of fiber-reinforced concrete is the most significant advantage. It should be considered when design the structures with UHPC. The studies to find the relationship between the material properties and the tensile strength are in active progress, but it is not defined yet. By testing and analyzing, the establishment of the post-cracking tensile relationship is necessary.

Two types of post-cracking tensile behavior model were proposed in MC 2010. The tensile strength when the crack occurs (P_{cr}) is

specified in both model. The behavior after it reached P_{cr} makes difference between two models.

The first type of post-cracking tensile behavior model is the softening model as shown in **Fig 1-1.** It has only one increasing tensile strength section after crack occurs. After it reaches its peak, the graph shows sharp fall for a while. The graph shows that it kept strength after small fall.

This phenomenon appeared due to the fiber's tensile strength. The first peak has shown as macro crack formed previously. The macro crack became the critical part, and it fails from this part. There is no more specific tension resistance at the other parts except for the critical failure section. The tension resistance is concentrated into this critical part. At the critical part the fibers can resist the tensile strength. That shows the maintenance of the tensile strength after the crack formation. It represents more ductile failure than the tensile failure of conventional concrete. However, the hardening model shows more ductile failure.

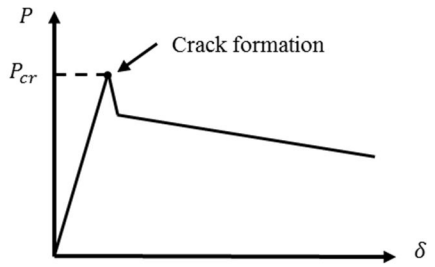

Fig 1-1. Softening Behavior in Axial Tension

The second post-cracking tensile behavior model is the hardening model shown in **Fig 1-2**. This model has increasing section after crack occurs. First increasing part appears before the crack formed, and the second increasing part is continued until the critical crack localization. After the second peak, the gradational drop of tensile strength has same shape with the softening model. The tensile strength is maintained with more deflection longer than in the softening model.

The second increasing part can be the most significant characteristic in UHPC tensile behavior. After matrix has formed the

micro-cracks, fibers control the tensile strength by bonding the matrix at the cracked section. As the fibers control the micro-crack section, diffuse micro-cracks are appeared on the specimen. It is called fiber effect. While the micro-crack spreads on the specimen due to the fiber effect, the tensile strength shows gradual increment. The slope is getting gentle, and it means that some micro-cracks are not able to resist the tensile force.

For this reason several types of fibers with different length are usually used. Shorter fibers have advantages on preventing the micro-crack, while longer fibers are used to avoid macro-crack more effectively. This principle was applied to the composition of K-UHPC, and two types of fibers with 16mm and 20mm are mixed.

The second peak appears with the crack localization. After critical crack has formed, the tensile behavior has same condition with the softening model. In this study the hardening behavior of UHPC is treated significantly to examine the punching shear failure considering the fiber effect.

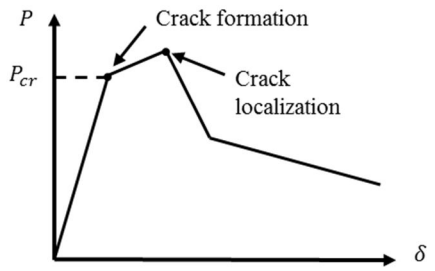

Fig 1-2. Hardening Behavior in Axial Tension

1.2 Advantage and Disadvantage of Using UHPC

There are many advantages when using UHPC for structural applications with its significant increment of strength compared to conventional concretes and even steel. Smaller sections and thinner structures are allowed by designing with high strength of UHPC. The smaller volume of structure leads to the use of less material to yield the same capacity.

The UHPC exhibits the significant improvements in tensile strength that has not been demonstrated in conventional concretes. This tensile strength allows the material to support to the loads both before and after the crack occurs. It prevents the brittle failure that would be common in a conventional concrete. K-UHPC code has demonstrated tensile strength as 13MPa. These tensile strengths were achieved as a result of the interaction of the steel fibers on the microscopic level and their ability to sustain load after the onset of cracking. By considering the effect of steel fiber reinforcement, the flexural and shear mild reinforcement can be reduced. The smaller reinforcement ratio results in the better durability. By using less reinforcement bars, it reduces the possibility of reinforcement rebar's corrosion.

The relationship of the ultimate punching shear strength and the slab depth was analyzed for the UHPC, FRC and RC slabs. As illustrated in **Fig 1-3**, the FRC and RC slabs did not show big difference. The RC slabs could not resist to the compressive force and the tensile force. Comparison with the FRC or UHPC, More steel reinforcement is necessary in RC slabs for intensifying the resistance force to the punching shear and the flexure. The slabs that are reinforced by the fibers have better punching shear strength than the slabs with same condition such as slab size, ratio of flexural reinforcement and the concrete compressive strength. However, the gap between the slabs made of similar condition of FRC and RC is smaller than the gap between the UHPC and RC slabs. Even though the UHPC slabs does not have the flexural reinforcement, the punching shear strength of UHPC slabs is much higher than that of FRC and RC slabs with same slab depth.

The tendency lines show that the increment of the ultimate punching shear strength according to the thickness of UHPC slabs will be much higher than the one of same thickness of FRC and RC slabs. Without flexural reinforcement the UHPC slab is predicted to have same or larger punching shear strength than the FRC or RC slabs of same thickness. Thicker UHPC slabs that are able to have axial reinforcement will have much higher resistance force to the punching shear and flexure. The thin slabs resisting high strength can be designed by using UHPC.

In this paper, 30mm to 60mm thickness of UHPC slabs were tested. The thin RC or FRC slabs are considered inappropriate to get the same ultimate punching shear strength with the tested UHPC slabs. The standard specifies that reinforcement system for satisfying the strength is not possible. It seems that there is the synergy effect with the fiber reinforcement and the high compressive strength in the increment of punching shear strength. For the thin structure that needs high strength, the UHPC seems the most proper material.

Nowadays, more architects try to design more unique form of architectures. For modern architecture, more thin structures will be requested. The UHPC can be a reasonable solution for the thin structures, while the RC could not be able to be reinforced due to the limitation of the slab depth and the design regulation. In this paper, seven slabs were tested to understand the performance of thin UHPC slabs.

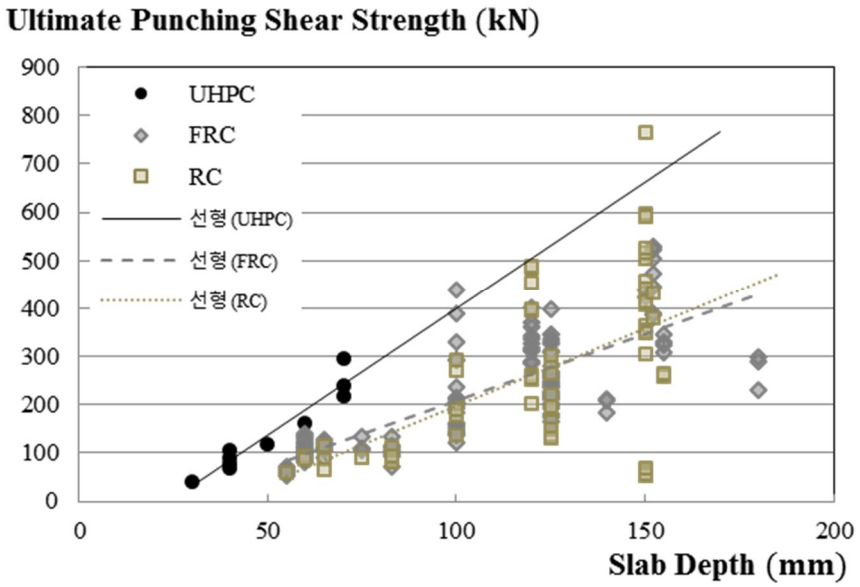

Fig 1-3 The ultimate punching shear strength according to the slab depth for the UHPC, FRC and RC slabs.

The biggest disadvantage of using UHPC is the initial cost. A limited number of UHPC structures are constructed. The design and use of the material has not yet been optimized and as a result, the cost is still

significantly higher than that of conventional concrete. If the construction of UHPC becomes more common in practice, the initial cost can be reduced significantly. The savings will be increased over the life cycle. Also to minimize the section properties of UHPC, design regulation should be confirmed by the structural tests. By more tests and applications, the regulation of limit how thin or small a member can be used. The serviceability is another issue with the ductility of UHPC.

The structural behavior of UHPC has not been determined completely. The punching shear behavior and equation are not defined due to the limited applications and test results of UHPC. To analyze the data only several papers were selected due to the application of different variables. To ensure the structural performance of UHPC as soon as possible, the guideline for material properties should be adopted first.

1.3 Research Strategy and Thesis Outline

The aim of this research is to accomplish a survey of the formulas suggested in previous literature that are dealing with punching shear capacity of UHPC slabs. Due to the lack of the practical UHPC structures and experiments, the fiber reinforced concrete structures are selected to examine the influence of the fibers. The data from the previous papers were analyzed to prove the validity of the equation and to understand the relationship between the material properties and the punching shear strength. Four papers that have the punching shear experimental data of fiber-reinforced concrete slab were chosen. The data extracted from the papers have differences with the experimental results from this paper. The first one is the compressive strength. While the UHPC in this paper has about 120MPa of compressive strength, FRC compressive strength data were only from 20 to 50MPa. The second one is the flexural reinforcement. Due to the lower strength of FRC, the reinforcement is essential. However, the final goal of this study is the application of UHPC as a thin plate. Very thin plate is insisted to utilize the thin UHPC slabs and the reinforcing structure that covers the RC slabs. Only un-reinforced UHPC slabs were tested, because it does not

have sufficient space for the flexural reinforcement. Also, the flexural reinforcement could not be used for confirming the performance of UHPC by itself.

After the first, introduction chapter, a survey of the literature is given. The literature survey was performed mainly for the estimation of the punching shear strength of fiber-reinforced concrete slabs. To reflect the main characteristic of the UHPC, the effect of the fibers is importantly considered.

In Chapter 3, the experimental data extracted from the four papers that has punching shear failure test results of the fiber-reinforced concrete were used for analyzing. The collected data were used for comparing the existing formula studied in Chapter 2.

Chapter 4 introduces the overview of the experiment process from the test setup to the measuring method. Chapter 5 gives the experimental results for comparing the formulas to find the most reasonable equation.

Chapter 2. Literature Review

2.1 ACI code

Punching shear failures occur from the formation of diagonal tension cracks around the loaded area, which result in a conical failure surface. A typical punching failure in reinforced concrete begins with the formation of flexural hinges around the perimeter of the loaded area. These hinges develop as a result of the moment caused in the slab by the applied load. This moment then begins to produce radial cracks that extend outward from the area of loading to the perimeter of the slab. Failure of the slab occurs when the diagonal tension cracks intersect the radial cracks and produce a cone of failure.

Based on the failure mode observed in typical punching shear failures, the concrete breakout failure mechanism results from an anchor pulling out of a concrete surface is considered to be indicative of tensile capacity since reinforcement is not considered. A number of models, in addition to the ACI code design equations for punching shear, were evaluated to determine if they were applicable for predicting the punching shear capacity of UHPC. From this procedure, it was regarded that it is not directly applicable to UHPC slab systems primarily as a result of the lack of reinforcing steel for flexure.

$$V_u \le \phi V_c$$

where,

V_u : the factored shear force on the slab system

ϕ : the strength reduction factor for shear $= 0.75$

V_c : the nominal shear strength provided by concrete

(V_c is the minimum of (2-1), (2-2), and (2-3))

$$V_c = (2 + \frac{4}{\beta_c})\sqrt{f'_c} b_o d \qquad \text{Equation (2-1)}$$

$$V_c = (\frac{\alpha_s d}{b_o} + 2)\sqrt{f'_c} b_o d \qquad \text{Equation (2-2)}$$

$$V_c = 4\sqrt{f'_c} b_o d \qquad \text{Equation (2-3)}$$

where,

f'_c : compressive strength of the concrete

b_o : the perimeter of the critical section

d : the effective thickness of slab

β_c : the ratio of the long side to the short side of the concentrated load or reaction area

α_s : a factor for slab column connections based on the location of the column (interior, exterior, corner)

2.2 K-UHPC code

K-UHPC code uses the tensile strength term that is calculated from a crack width-tensile stress graph (**Fig. 2-1**). The simplified tensile softening curve in the code is drawn by the direct tensile experiments. The test method is defined in K-UHPC code. The notched specimens were tested with the clip gauge on the side of it. The specimens are installed to the longitudinal direction. The prevention of partial disposition is important in the direct tensile strength test. After the crack is shown on K-UHPC, the tensile strength of the specimen is increasing gradually. The increment of crack width causes the increment of tensile strength of the fibers. After the tensile strength reached the peak point, it reduces slowly until the crack width reached the point that transference of the tensile stress is not made any more.

The specific material properties and the proportion of K-UHPC are used to manufacture the specimens. The diameter of the fibers is equal to 0.2mm. 16mm and 20mm length of fibers are mixed in a ratio of 1% each. The crack width w_u when the tensile strength has revealed is defined as 0.3mm. From the experiment, the tensile strength has not been reached when the crack width is smaller than 0.3mm, so it is

suitable for the safety reason. AFGC-SETRA regulation also defined the strength when the crack with is 0.3mm as the limitation of the tensile strength. The crack width that there is no more tension resistance, $w_{\lim}$ was suggested as 5.3mm, from the experimental results.

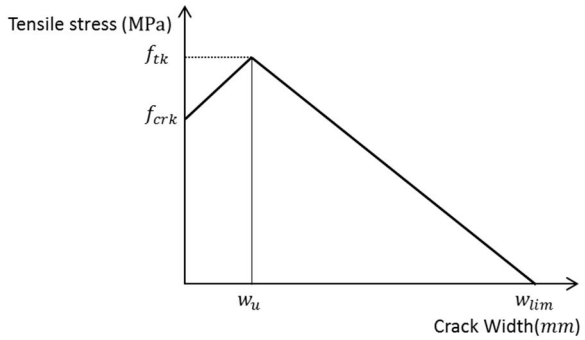

Fig. 2-1. Crack Width – Tensile Stress Diagram

For the K-UHPC that follows the composition in K-UHPC code and the method of curing, the tensile strength, f_{crk} when the crack has occurred is determined to 9.5MPa. When the crack width is 0.3mm, the tensile strength f_{tk} is 13.0MPa. However, adopting this graph to the estimation of punching shear has problem that it could not consider the material properties.

$$V_{pcd} = \phi_b f_{vd} u_p d$$

where,

ϕ_b : Member reduction coefficient (generally, 0.77)

f_{vd} : Average tensile strength of K-UHPC on the orthogonal direction to the diagonal crack

$$f_{vd} = \frac{1}{w_v}\int_0^{w_v} \phi_c \sigma_k(w)\, dw$$

$w_v = \max(w_u, 0.3mm)$

w_u : Crack width when the maximum stress reached

$\sigma_k(w)$: Tensile stress-crack width diagram (**Fig. 2-1**)

d : Depth of the slab

u_p : The perimeter of the critical section located at a distance of $d/2$ from the edge of the loading pad

The code equation predicts the punching shear strength based on the relationship of the crack width and the tensile stress. It leads to the result that the serviceability and the failure mode can be applied easily. The critical section is assumed same with the critical section of conventional concrete flat plate. UHPC flat plate is expected to fail on the wider section, so the improvement of the study on critical section of UHPC flat plate and the failure behavior is essential. The code only considers the shear strength of matrix, and the shear strength of reinforced bar is not considered.

2.3 Fib Model Code 2010

The punching shear failure mode that Muttoni suggested was divided into three types. First one is cantilever action shown in **Fig 2-1 (a)** that makes new internal load bearing action when the crack blocks the stress path, so there is no load transfer over the cracks. The cracks divide the concrete elements, and it seems like a cantilever beam fixed in the upper compression zone. Second, interlocking action (**Fig 2-1 (b)**) is the action like friction that the concrete compression delivered through the rough side of the crack, and it is related to the aggregates' size. In UHPC, since the maximum size of the aggregate is very small, the interlocking action can be ignored. For the last, transverse reinforced rebar deforms more as the crack becomes wider. The Rebar connects the tensile stress path even after it deformed. Deformed rebar delivers the stress also to the vertical direction not only to the horizontal direction. It is called dowelling action (**Fig 2-1 (c)**). UHPC is developed not to use the reinforcement, so the equation considering the effect of reinforcement separately with the concrete's is to be developed.

$$V_{R,c} = \frac{3/4}{1+15\cdot\frac{\psi\cdot d}{16+d_g}}\cdot b_o \cdot d \cdot \sqrt{f'_c}$$

where,

ψ : The rotation angle of the slab

$$\psi = 1.5\cdot\frac{r_s}{d}\cdot\frac{f_{yd}}{E_s}\cdot\left(\frac{m_{sd}}{m_{Rd}}\right)^{1.5}$$

d_g : The maximum aggregates' size (for UHPC, 0)

b_o : The perimeter of critical section ($1/2\cdot d$ far from the loading area)

d : Slab thickness

f'_c : Compressive strength of concrete

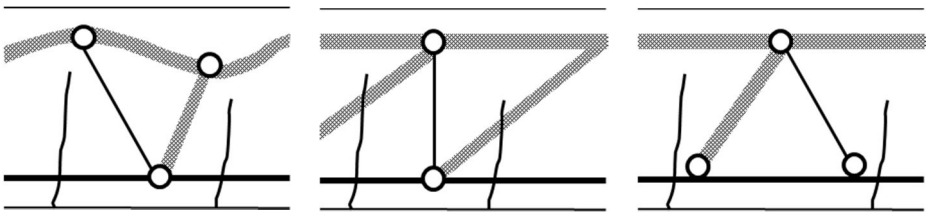

(a) Cantilever action (b) Interlocking action (c) Dowelling action

Fig 2-1. Structural Models after Bending Cracks Develop with Subsequent Crack Propagation (Muttoni and et al, 1991)

Muttoni suggested a punching shear failure model based on several assumptions. Concrete is assumed as rigid body after failure. The maximum crack width occurs on the tension side of the point that has theoretical location of the strut as shown in **Fig 2-2**. After the slab rotated, the crack width is proportionally getting wider to the tension side of the slab. This leads to the point that the crack width is proportional to the rotation angle and the slab depth. The punching shear strength is inversely proportional to the crack width, so the equation has the rotation angle and depth term on denominator. The rough failure

section causes the interlocking action, so it has d_g term that stands for the aggregate size. Dowelling action caused by the flexural reinforcement is neglected due to the spalling of the concrete cover.

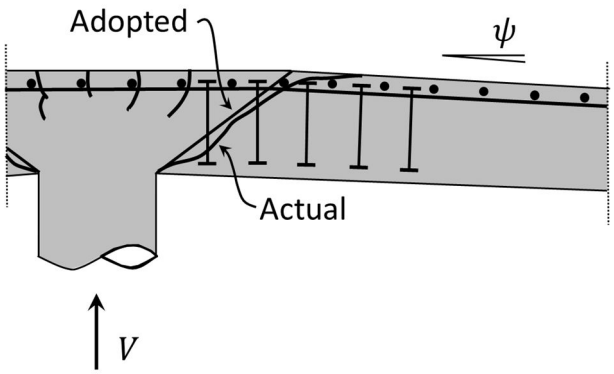

Fig 2-2. Punching shear strength in shear-reinforced slabs based on critical shear crack theory: actual and adopted geometry for critical shear crack localizing strains (Miguel and et al., 2009)

2.4 KCI code 2012

KCI code concludes several coefficients such as k_s, slab thickness coefficient and k_{bo}, the effect of critical section perimeter coefficient. Also, KCI code considers f_{te} that represents the tensile strength at the compression zone in the concrete. The empirical formula $v_c \approx (1/3)\sqrt{f_{ck}}$ was determined for predicting the punching shear strength at the two-way bending slab that only considers compressive strength. However, it could not predict the punching shear strength properly, especially with lower flexural reinforcement ratio. To determine the shear strength at the compression zone more accurately, the combined strength of shear strength and the bending moment should be considered. For this reason, the formula $f_{te} = \cot\varphi (= \sqrt{f_{te}(f_{te} + f_{cc})}$ is induced.

$$V_c = v_c\, b_o\, d$$

$$v_c = \lambda k_s k_{bo} f_{te} \cot\psi (c_u / d)$$

where,

$$k_s = (300/d)^{0.25} \le 1.0$$

$$k_{bo} = 4/\sqrt{\alpha_s (b_o / d)} \le 1.25$$

$$f_{te} = 0.21\sqrt{f_{ck}}$$

$$\cot\psi = \sqrt{f_{te}(f_{te} + f_{cc})} / f_{te}$$

$$c_u = d[25\sqrt{\rho / f_{ck}} - 300(\rho / f_{ck})]$$

$$f_{cc} = (2/3) f_{ck}$$

2.5 Swamy and Ali (1979)

Swamy and Ali performed test of the slab-column connections made with steel fiber concrete. The nineteen test specimens were full-scale models of flat slab structures, and five of them do not have fiber reinforcement. For studying the different variables, the specimens were divided into five series. The series one and three had different fiber volume percentage and the fiber types each. In second series, fiber location and flexural reinforcement distribution was varied. Series four has the specimens with the reinforcement reduction. The specimens with variation of shear reinforcement were the main studied variable in fifth series.

From experiment, by loading the sub column centrally and beyond the maximum load, the descending post-peak curve was obtained. The researchers elucidated that fibers increased the ultimate punching shear loads, as well as when doubling the fiber volume ratio content the maximum load improved about 30 percent. To concentrate the fibers inside the distance of three times of the thickness of the slab from the column faces over the full slab depth confirmed to be as effective as providing fibers in the whole slab depth. They estimated that hooked fibers were more efficient than plain fibers, but less effective than

crimped fibers. Crimped fibers had better deformation resistance and increased punching shear capacity, ductility, and energy absorption capability. Nowadays, the crimped fibers are used in UHPC.

They did not concentrate only on the punching shear strength, and carefully observed the deflection and the failure behavior of the FRC slabs. The concrete strains on the top and bottom side of the slabs allows confirming the critical part of the slabs. The punching behavior of the slabs is the one of the most important aims to figure out. Due to the brittle behavior of punching shear failure, the deflection or failure patterns could be difficult to be defined and lead to the subjective analysis. Therefore, the observation of deflection was carefully examined.

2.6 Narayanan and Darwish (1987)

The effects of steel fiber reinforcement on the punching shear capacity of fiber-reinforced concrete without coarse aggregate are studied by Narayanan and Darwish. The test variables in their investigation were fiber volume ratio, amount of tensile reinforcement, and concrete strength. In their study, a total of twelve slabs were tested to failure, and illustrated the improvement achieved in punching shear capacity with steel fiber contents. The results indicated that an increment of fiber volume ratio improved the punching shear strength and modified the position of the critical perimeter. They also developed an equation that was based on a semi-empirical model for estimating the ultimate punching shear strength of fiber-reinforced concrete.

$$v_u = \xi_s (A' f_{spf} + B'' \rho + v_b)$$

where,

f_{spf} : Computed value of split cylinder strength of fiber-reinforced concrete, $(\mathrm{N/mm^2})$

$$f_{spf} = \frac{f_{cu}}{20} + 0.7 + \sqrt{\frac{\rho_f d_f L}{D}}$$

f_{cu} : Compressive strength of cube concrete

ρ : Area of tensile reinforcement

v_b : Vertical fiber-pull-out stress along the inclined crack

$$(\mathrm{N/mm^2}) = 0.41\tau F$$

τ_u : Average bond stress on the fiber surface (4.15MPa)

$F = (\frac{L}{D})\rho_f d_f$: Pull-out strength at the diagonal crack caused by fibers

L : Length of fiber

D : Diameter of fiber

ρ_f : Volume fraction of fibers

d_f : Bond factor

This equation has the difference from the previous ones that it calculates the strength of concrete, reinforcement and fibers separately. The separate consideration of each term allowed for the punching shear capacity of UHPC slabs to be compared by neglecting the contribution of the tensile reinforcement. The contribution by the concrete in the first term, the tensile reinforcement in the second term, and the steel fibers in the third term can be distinguished. Especially in this equation, the pull-out strength related to the bond factor and fiber factor is included, and it is helpful to apply the material properties that the other equations did not consider. In order to use this equation, the term that represents the tensile steel contribution was not included because no tensile reinforcement was used in this experiment. Also, this equation is semi-empirical formula so that the coefficients for each term are from experimental data. With the other material properties the gaps between the test results and the predicted results are relatively large. To complement this problem, more material experiments that lead to the constitutive law are necessary.

The split cylinder strength of fiber-reinforced concrete is contained in the equation. Not all the experiments include the split cylinder tests for the material property determination. So, Narayanan and Darwish

adopted the calculated split cylinder strength value to substitute for the equation. The compressive strength of the cube concrete reflects the strength of the matrix. The last term is applying the effect of fibers that affect the tensile strength of the UHPC. By comparing the equation with the other equations, the influence of adopting the split cylinder strength of fiber-reinforced concrete can be defined.

2.7 Shaaban and Gesund's equation (1994)

Shaaban and Gesund tested thirteen reinforced concrete slabs with the variable of strength and the amount of fibers. The aim of their experiment was to determine if the punching shear capacity could be improved through the addition of fibers. Their research was based on the previous researches that indicated that the reinforcement of fibers to concrete increased the tensile capacity. The increased tensile strength is directly related to punching shear, so they expected containing fibers would have effect on the punching shear strength. The analysis focused on the critical punching area.

They proposed an equation of the same form as the ACI 318-02 code equation for punching shear. Some modifications were applied to account for the fiber contribution. The advantage of this equation is that it maintains the general form of ordinary used code equations. However, for substituting to the equation, most of the papers do not consider the variation of the percent of fibers by weight of concrete. Usually the fiber volume ratio is adopted for material verification of UHPC, the modification of the application of the percent of fibers by weight is necessary.

$$V_c = [(0.3 \cdot W_f + 6.8) \cdot \frac{\sqrt{f'_c}}{1000}] \cdot b_o \cdot d \quad \text{(kips)}$$

where,

W_f : Percent of fibers by weight of concrete (%)

f'_c : Concrete compressive strength (psi)

b_o : Critical perimeter as defined by ACI (in.)

d : Average effective depth to tension reinforcement (in.)

2.8 AFGC Code for Ultra High Performance Concrete

This equation has almost same form with the K-UHPC equation with new term considering directivity of the fibers. The directivity of the fibers is determined according to the location of the concrete.

$$V_{pcd} = 0.8 \frac{f_{ct}}{K_{local} \times \gamma_{cf}} u_p d$$

where,

K_{local} : Directivity of the fibers

$f_{ct} = \min(f_{ctfk}, f_{ctk,el})$

f_{ctfk} : The maximum post-cracking tensile strength

$f_{ctk,el}$: Tensile strength at elastic limit

u_p : The perimeter of the critical section located at a distance of $d/2$ from the edge of the loading pad

2.9 JSCE

Japanese Code, JSCE is similar to the Narayanan's equation and it considers the effect of concrete and fibers individually. The difference is the concrete and reinforcement in one term, V_{pcd}. The fiber effect V_{pfd} is calculated separately. Narayanan equation considers the fiber's effect in the split cylinder strength of concrete, while JSCE code equation calculates the reinforcement in the matrix term. Another characteristic of this equation is that it considers the tensile strength of the concrete in V_{pfd} term. The tensile strength of UHPC is the one of the main characteristics, and it considerably affects punching shear strength. The

direct tension tests should be done for the material tests in the structural experiment. With this reason, the application of the direct tensile strength is worthy of notice.

$$V_{pd} = V_{pcd} + V_{pfd}$$

where,

$$V_{pcd} = \sqrt[4]{1/d} \cdot \sqrt[3]{100\rho} \cdot (1 + \frac{1}{1 + \frac{0.25u}{d}}) \cdot f'_{pcd} \cdot \frac{u_p d}{\gamma_b}$$

$$V_{pfd} = f_{vd} \cdot \frac{u_p d}{\gamma_b}$$

$f_{vd} = f_{tk} / \gamma_c$: Nominal tensile strength

f_{tk} : Tensile strength

γ_b : Safety factor (=1.3)

u : the perimeter of the loading area

u_p : The perimeter of the critical section located at a distance of $d/2$ from the edge of the loading pad

ρ : Reinforcement ratio

In this study, the test specimens are K-UHPC slabs have no flexural reinforcement. Therefore, the concrete term V_{pcd} is not considered, because the reinforcement ratio of the UHPC slabs is zero. For the experimental results that were performed in this paper the fiber effect is only considered. The fiber term, V_{pfd} shows similar form with the ACI code equation. It shows very simple form that only contains nominal tensile strength, safety factor, and critical section term. By applying this equation, the relationship between the tensile strength and the punching shear strength is expected to be found.

The critical section term in the equations above is same for $u_p d$. It assumed the critical section has occurred at a distance of $d/2$ from the edge of the loading area. It means that the assumption of the critical crack angle is same with the conventional concrete slab. However, the UHPC or fiber-reinforced concrete is expected to fail in lower slope. The fibers bond the matrix after the micro-cracks occur, and the matrix can

spread the compressive stress to the wider section. That is the reason the gentle strut angle is expected in the UHPC. It will allow the increment of punching shear strength in slab, larger than that of tensile strength in direct tension tests. Fiber components such as the directivity of fibers and the fiber volume ratio will affect the critical section, and need to be observed.

Chapter 3. Preliminary Analysis

3.1 Summary of preliminary analysis procedures

Two differences between the conventional concrete and the UHPC are the high strength and the flexural reinforcement. In this study, the experimental data obtained from the fiber-reinforced concrete slab testing is collected for analyzing to understand the effect of the fibers on UHPC. **Table 3-1** has the experimental data that is extracted from four papers. Not many papers could be selected due to the application of different variables. Some of the papers could not be adopted in the equations by stating the percent of fibers by weight of concrete instead of fiber volume ratio, or no specification of the tensile strength of FRC. To ensure the structural performance of UHPC as soon as possible, the guideline for material specification should be adopted first.

The first paper "Punching shear tests on steel-fiber- reinforced micro-concrete slabs" written by Narayanan and Darwish, second, "Punching shear strength of steel fiber reinforced concrete slabs" written by Tan, Third "Punching shear behavior of reinforced slab-column connections made with steel fiber" written by Swamy and Ali, and the last "Design equation for punching shear capacity of SFRC slabs" written by Higashiyama are chosen for analyzing. The main variables such as fiber volume ratio (ρ_f), compressive strength of concrete (f'_c), flexural reinforcement ratio (ρ), and slab depth (d) are entered to get the results calculated from the equations that are handled in the previous chapter. For the results from the same value of variable in each paper, only the maximum and minimum results are selected not to get the concentrated results. The selected results are sorted according to the fiber volume ratio (ρ_f) and the compressive strength of concrete (f'_c).

Table 3-1.Comparison of the existing formulas

	ρ_f [%]	d [mm]	f'_c [MPa]	V_{test} [kN]	ACI [kN]	MC 2010 [kN]	KCI [kN]	Narayanan [kN]	JSCE [kN]
Narayanan and et al. (1987)	0	45	43.28	86.5	62.52	76.74	121.41	69.32	115.07
	0.25	45	52.08	93.4	68.59	84.18	130.82	89.51	126.23
	0.5	45	44.72	102	63.56	78.01	123.06	91.72	116.97
	0.75	45	46	107.5	64.46	79.12	124.48	96.23	118.63
	1	45	52.96	113.6	69.16	84.89	131.68	99	127.29
	1.25	45	53.04	122.2	69.22	84.96	131.76	92.64	127.38
	1	45	46.96	92.6	65.13	79.94	120.66	94.4	115.32
	1	45	45.28	111.1	63.95	78.49	128.11	96.03	122.02
	1	45	43.52	111.3	62.7	76.95	129.65	96.34	123.42
	1	45	47.6	113.3	65.57	80.48	138.51	99.89	132.98
	1	45	29.76	82.1	51.84	63.63	103.10	86.05	95.421
	1	45	32.4	84.9	54.09	66.4	107.18	87.51	99.56
Kiang-Hwee and et al. (1994)	0.31	21.8	40	21.4	22.34	21.02	35.61	25.61	37.84
	0.31	21.8	40	22.6	22.34	16.29	35.61	25.62	37.84
	0.31	21.8	40	18.9	22.34	13.32	35.61	25.61	37.84
	0.5	21.8	40	20.9	22.34	16.29	35.61	27.68	37.84
	1	21.8	40	23.7	22.34	16.29	35.61	31.08	37.84
	1.5	21.8	40	24.6	22.34	16.29	35.61	31.91	37.84
	2	21.8	40	27.4	22.34	16.29	35.61	30.32	37.84
	0.31	13.7	40	9.4	10.96	9.24	16.87	13.4	24.01
	0.31	35.5	40	54.9	46.54	30.87	79.82	53.56	63.76
	0.31	43.6	40	70.5	61.89	40.97	110.09	74.38	80.66
	0.31	21.8	28	19	18.69	13.63	31.35	21.84	31.66
	0.31	21.8	52	20	25.47	18.57	38.92	29.39	43.15
	0.31	21.8	40	26.1	31.5	28.36	46.99	39.66	65.35
	0.31	21.8	40	18.7	26.92	22.33	41.69	32.63	51.61

	ρ_f [%]	d [mm]	f'_c [MPa]	V_{test} [kN]	ACI [kN]	MC 2010 [kN]	KCI [kN]	Narayanan [kN]	JSCE [kN]
Swamy (1984)	0	110	36	197.7	239.58	191.85	245.28	210.44	223.35
	0.6	110	36	243.6	239.58	191.85	245.28	353.1	223.35
	0.9	110	36	262.9	239.58	191.85	245.28	367.9	223.35
	1.2	110	36	281	239.58	191.85	245.28	353.15	223.35
	0.9	110	36	267.2	239.58	191.85	245.28	367.9	223.35
	0.9	110	36	239	239.58	191.85	245.28	367.9	223.35
	0	110	36	221.7	239.58	191.85	245.28	210.44	223.35
	0.9	110	36	236.7	239.58	191.85	245.28	341.31	223.35
	0.9	110	36	249	239.58	191.85	245.28	367.9	223.35
	0.9	110	36	262	239.58	191.85	245.28	367.9	223.35
Hiroshi and et al. (2011)	0.67	70	24.6	137.5	91.65	85.42	153.89	138.35	111.89
	0.67	110	24.6	210.2	172.84	161.08	218.07	267.08	175.25
	0.67	150	24.6	297.6	274.97	256.26	317.33	435.5	245.5
	0.72	65	42.4	140.8	111.73	104.13	192.16	160.36	136.8
	0.72	105	42.4	213.2	216.59	201.86	266.86	320.01	219.77
	0.72	145	42.4	290.7	348.96	325.22	378.75	529.48	309.51
	0.91	65	21.6	120.8	79.75	74.32	149.82	134.62	97.64
	0.91	105	21.6	183.1	154.59	144.08	212.78	267.27	156.86
	0.91	145	21.6	231.2	249.07	232.13	303.52	441.09	220.91
	0.63	70	27.8	152.3	97.43	90.8	161.08	141.99	118.94
	0.94	70	31.1	147.9	103.05	96.04	167.80	160.81	125.81
	1.03	70	30.4	158.9	101.89	94.96	166.43	162.68	124.38

3.2 Tendency Analysis for Fiber Volume Ratio

Fig 3-1 is the graphs by sorting the results calculated from the punching shear equations according to the fiber volume ratio. The ACI code, fib Model Code 2010, JSCE code equations and the equation that Narayanan and Darwish suggested are employed. From each paper, the maximum and minimum results with same fiber volume ratio were extracted to avoid the concentrated results, and to understand the relationship between the fiber volume ratio and the equation accuracy.

The JSCE code and Narayanan equation consider the fiber volume ratio, while the other code equations do not include the term related to the fiber effect. With that reason, the arrangements of the ACI code and MC 2010 results are decentralized higher than those from Narayanan equation or JSCE code. ACI code and MC 2010 shows that nine and eight outcomes each represent larger value than 1.5, and most of the dots are above the dotted line that represents the 1. This phenomenon leads to the result that the ACI and MC 2010 underestimate the punching shear strength of FRC. The ascending trend lines are shown in ACI code and MC 2010. With more fiber contents the punching shear strength is getting higher, but the code equations that do not consider the fiber effect could not reflect the increment of punching shear strength.

The trend line shows that the JSCE code predicts the punching shear strength the most closely to the experimental data. The JSCE code has one data below the 0.5, while the Narayanan equation does not have. The inclinations of the trend line from Narayanan and JSCE code equations are gentler than the others. It shows that the Narayanan and JSCE code equations are applied well with the reflection of the fiber effect. The most of the results have shown near the dotted line representing 1. For economical FRC slab design, the Narayanan or JSCE code should be adopted.

KCI code equation predicts the punching shear strength better than the others. The KCI code results have the smallest standard deviation, but it tends to overestimate the ultimate strength the most. The slope of increased tendency line seems not larger than the other RC code equations.

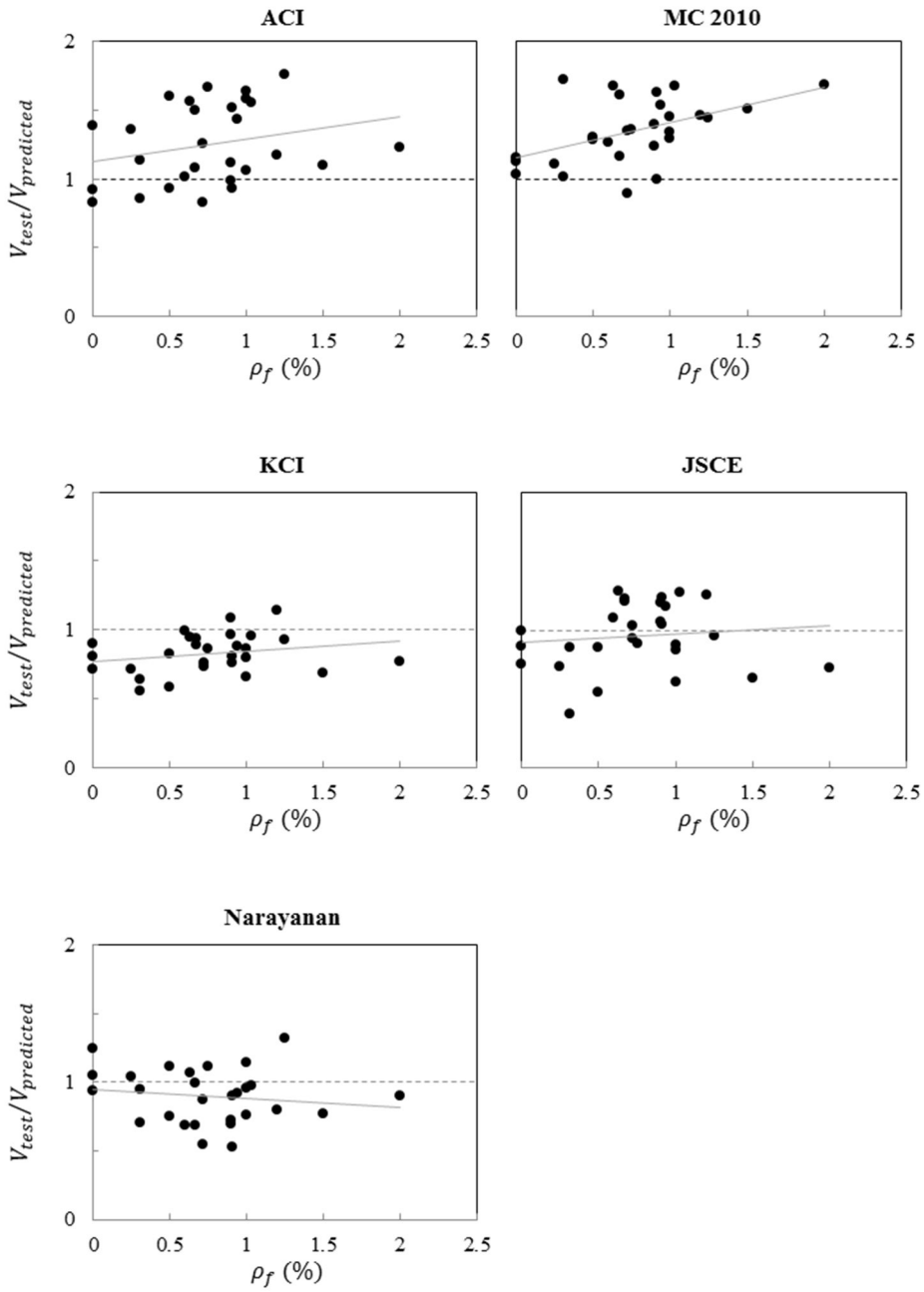

Fig 3-1. Comparison of the Formulas according to the Fiber Volume Ratio

Table 3-2. Distribution on Fiber Volume Ratio

Equation	Average	Standard Deviation
ACI code	1.252	28.6%
MC 2010	1.346	22.8%
KCI code	0.829	13.9%
Narayanan	0.899	19.7%
JSCE	0.954	23.4%

Table 3-2 shows that the Narayanan's equation, the JSCE code and KCI code equation have the $V_{experimental} / V_{predicted}$ value less than 1. This means that these equations overestimate the punching shear strength of the slab. To get the safe and reasonable results the safety factor can be adopted. In addition, KCI code equation results have the smallest standard deviation among five equations' results. However, the equation that the results are the closest was JSCE code, the error was about 5% only. From this, the method that calculates the fiber term and the matrix term separately can be accurate for predicting the punching shear strength according to the fiber volume ratio. The Narayanan's calculation method of strength caused by fiber's effect can be better than the other equations. More experiments to analyze the effect of the other fiber properties such as diameter, length, and shape of the fibers are needed.

3.3 Tendency Analysis for Compressive Strength of Concrete

The graphs illustrated in **Fig 3-2** have been come out by arranging the data into the compressive strength of concrete (f'_c) order. From each paper, the maximum and minimum results with same compressive strength were extracted to avoid the concentrated results, and to understand the relationship between the fiber volume ratio and the equation accuracy.

The ACI code equation and MC 2010 equation contain the compressive strength of cylinder concrete term ($\sqrt{f'_c}$). For the consideration of FRC performance on tensile strength, Narayanan's equation contains the split cylinder strength term (f_{spf}). The nominal tensile strength term (f_{tk}) is applied in the JSCE code equation. The application of split cylinder strength and the tensile strength should be compared to the application of compressive strength of concrete.

The result arrangements from the ACI code and MC 2010 shows that thirteen and six outcomes each represent larger value than 1.5, and most of the dots are above the dotted line that represents the 1. However, the inclinations of trend lines shown in ACI code and MC 2010 were gentler than the other equations.

The Narayanan and JSCE code equations that are considering the fiber effects predict the punching shear strength better than the other equations. However, the errors in accordance with the compressive strength were shown larger than the upper two equations. The application of compressive strength term directly results in more stable drift. Narayanan's equation is regarded to be made up for the weak point that tends to underestimate of the punching shear strength made of high compressive strength FRC. The JSCE code results drift shows the opposite tendency with the Narayanan's equation results. The application of the split cylinder strength, or tensile strength in FRC estimates the punching shear strength better than the others. However, the MC 2010 shows the most stable tendency among the four equations. Unstable drift curves that were shown in below two graphs can lead to a wrong estimation with high strength of concrete especially the UHPC. The consideration of adopting compressive strength should be studied in further study, for proper estimation of the high strength of FRC.

Table 3-3. Distribution on Compressive Strength of Concrete

Equation	Average	Standard Deviation
ACI code	1.396	29.8%
MC 2010	1.337	22.8%
KCI code	0.806	13.0%
Narayanan	0.969	19.6%
JSCE	0.965	20.7%

From **Table 3-3**, Narayanan and JSCE code equations are the most proper prediction. The results from these two equations have the smallest standard deviation and the closest results to the tested value. In compressive strength order, Narayanan and JSCE show very similar results. From this result, it shows the application of split cylinder strength or the tensile strength does not affect the estimation of punching shear strength. More experiments to analyze the effect of the application of strength term such as split cylinder strength, tensile strength and the square root of compressive strength.

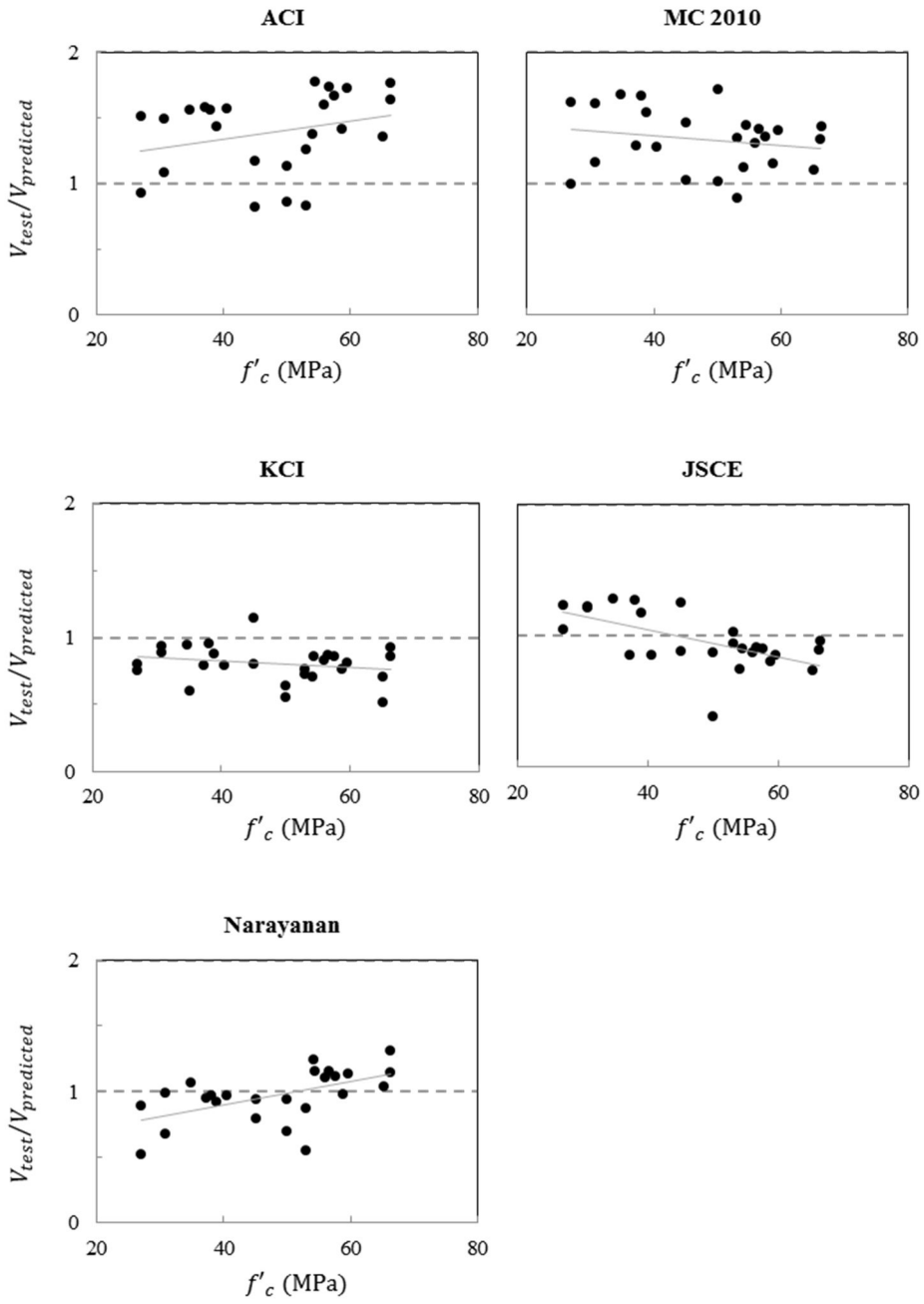

Fig 3-2 Comparison of Formulas according to the Compressive Strength of Concrete

3.4 Comparison of the Predicted Results and the Experimental Results

Overall comparison of the predicted results and the experimental results are illustrated in **Fig 3-3**. The drift curves of ACI code and MC 2010 are more stable than the other two drift curves below. However, two code results above show the different aspect each other. The ACI code result shows the arrangements are grouped in three parts, according to the experimental results. For the results from the other papers, the accuracy ratio seems totally different. The experimental results and predicted ratio ($V_{test} / V_{predicted}$) seems very accurate for the specimens with low and high punching shear test results. For the specimens that the tests results are between 100 and 200, the equation tends to underestimate. In case of MC 2010, the overall tendency of each paper's results seemed similar. The MC 2010 results are not affected by the material properties, while the ACI results seem that they are. The application of the slab rotation angle is very subjective, while there is no specific definition. The failure mode that Muttoni suggested defines that the slab rotation angle can be calculated from the center to the boundary with the biggest deflection to the downwards. It was more applicable than the simple ACI failure mode. To be applied in the FRC slabs or the UHPC slabs, new definition of failure mode and the deformation should be needed.

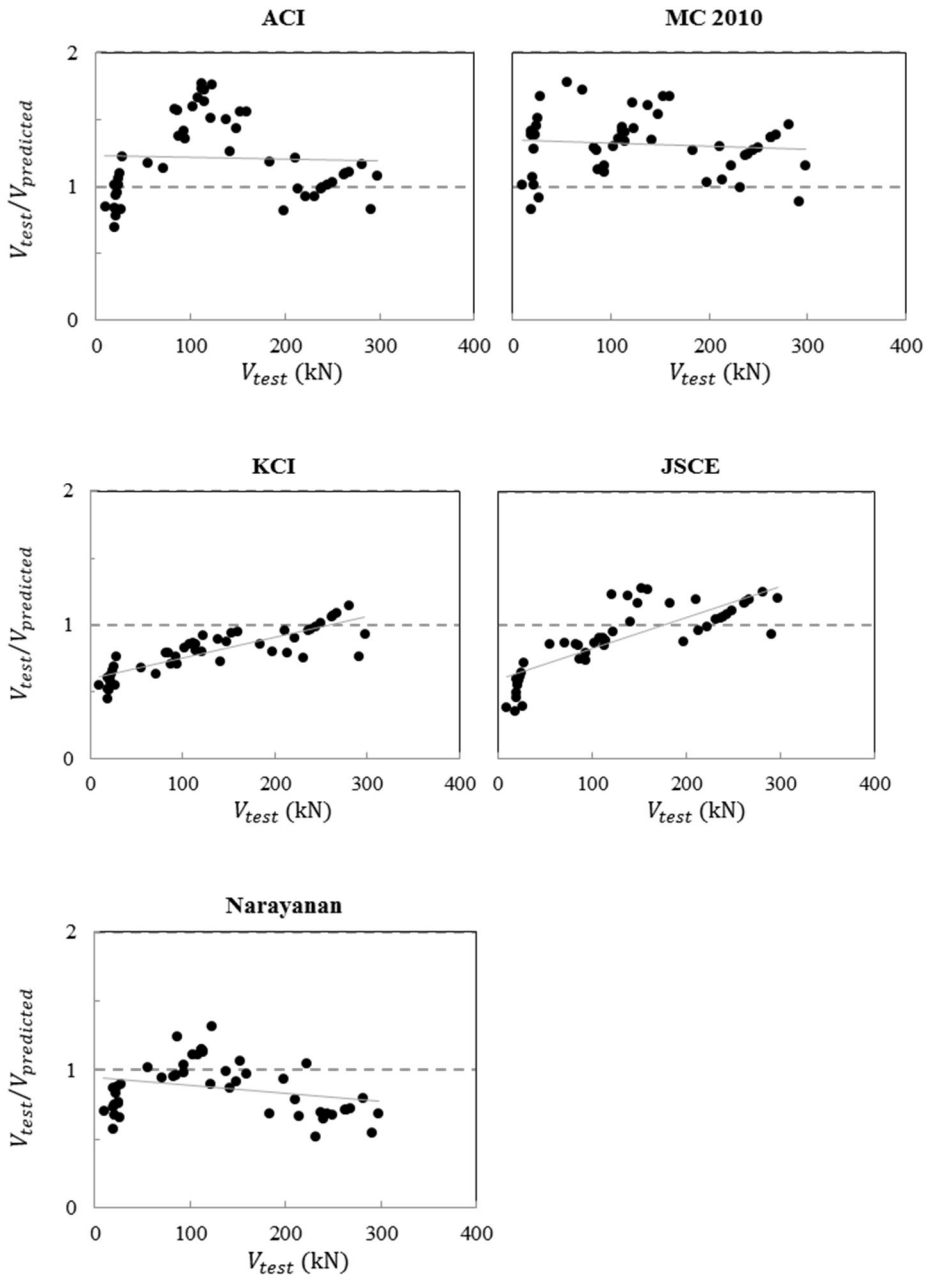

Fig 3-3 Comparison of Existing Formulas

The overall tendencies of each paper's results in Narayanan and JSCE was not dispersed as much as that the ACI tendency shows, but not analogous as much as that the MC 2010 tendency shows. Especially, it seems that the Narayanan's equation results are less affected by the papers' diversity than the JSCE does. The JSCE code equation has inclined trend line, so the reason of grouping of the result arrangements is not proved positively. There is another possibility that the JSCE tends to underestimate the slab performance with high strength. By analyzing more data the reason of this problem should be defined.

Table 3-4 Distribution on Predicted Results

Equation	Average	Standard Deviation
ACI code	1.213	30.2%
MC 2010	1.316	22.3%
KCI code	0.805	16.3%
Narayanan	0.869	19.3%
JSCE	0.901	25.8%

In **Table 3-4** and **Fig 3-4**, Narayanan's equation and JSCE code equation have the closest results with the experimental results. The equations calculating matrix and fibers' strength individually are more reasonable. When concrete, reinforcement and fibers' strength are calculated separately, the coefficients of each terms are usually determined by experiments. For certain material property, it shows only slight gap between the experimental value and the predicted value, but for other material properties it shows big gap. That is why the relationship between the material properties and the punching shear strength is needed to be examined.

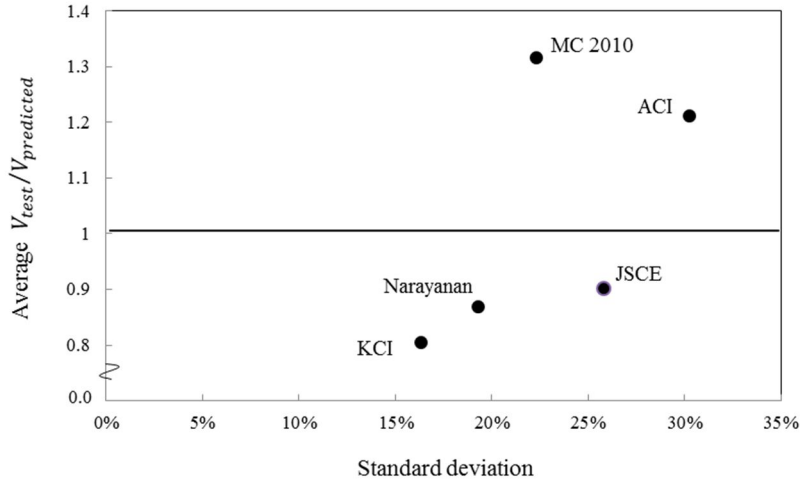

Fig 3-4 Average and Standard Deviation of Ratio of Tested Strength to Predicted Strength by Existing and Code Equations

Chapter 4. Materials and Testing

4.1 Fabrication

4.1.1 K-UHPC

Mixing proportion of K-UHPC is like as **Table 4-1.** The ordinary Portland cement and silica fume is used in K-UHPC as cement and reactive power. The fine aggregates used in K-UHPC with diameter smaller than 0.5mm are SiO_2 content larger than 96%. The average particle size of filler shall be 4μm. The tensile strength of steel fibers shall basically be over 2,000MPa.

The characteristics of the composition of K-UHPC are lack of coarse aggregate and the low volume of water. Water-cement ratio of the K-UHPC is 0.23. High proportion of cementitious materials and low volume of water minimize the space between the particles. The fine sand is filled in the remainder of space.

The strength of the reinforced fiber is 2500MPa. The 19.5mm long fibers and 16.3mm long fibers are mixed in the ratio of 2:1. The tensile strength of UHPC is the main character that should be considered for designing structures. However, the relationship of the amount of fibers and the structural performance has not been approved. To observe the effect of fibers, four types of steel fiber volume ratio were selected. The fiber volume ratio is from 0% to 1.5%.

Table 4-1 UHPC Mixing Composition

W/B (%)	Cement (kg/m^3)	Silica fume (kg/m^3)	Sand (kg/m^3)
23	783.2	195.8	861.52
Filing powder (kg/m^3)	Superplasticizer (kg/m^3)	Steel fiber volume ratio	
234.96	15.66	0%~1.5% (19.5mm and 16.3mm fibers are mixed in the ratio of 2:1)	

The seven slabs used in the testing were fabricated. **Fig 4-1** shows the process of fabricating the specimens. The formwork was constructed to produce $1{,}600mm \times 1{,}600mm$ slabs as illustrated in the **Fig 4-1 (a-c)**. To fix the specimens to the experimental jig easily the holes were torn by installing the cylinders. Two lifting eyes were installed on the opposite side in the corner location to allow easy lifting and positioning of the slabs. The slabs with four types of fiber volume ratio from 0% to 1.5% were constructed for the testing object. The 19.5mm long fibers and 16.3mm long fibers were inserted in the ratio of 2:1 as shown in **Fig 4-1 (d)**. The fibers and other compositions were compound in the mixed machine, in **Fig 4-1 (f)**. Since UHPC shows remarkable workability performance, it flows down to the form easily. The forms do not have the lid, and the natural forming can be expected (**Fig 4-1 (e-f)**). The flowing UHPC results in the natural shaping and good construct ability. However, it shows prints as passing between the small formwork articles. There is a problem that the directivity of fibers could not be predicted easily.

(b) Part of jig

(a) Form

(c) Detail of form

(d) Fibers

(f) View of laboratory

(e) Pouring UHPC

(g) Setting horizontal

(h) Detail of specimen

Fig 4-1. Process of Fabrication

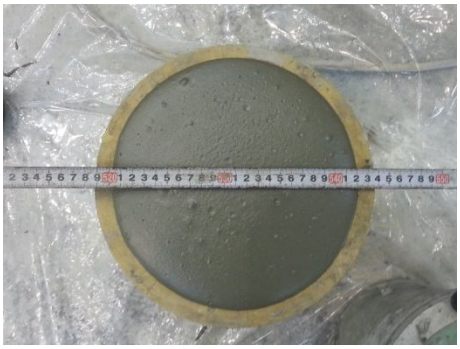

(b) Slump test

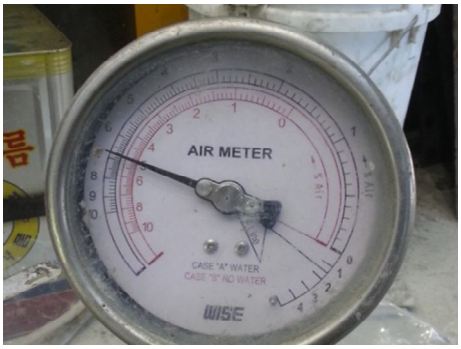

(a) Air content test

(c) Curing in lab

(d) Tension test specimens

Fig 4-2. Concrete Test of K-UHPC

Regardless of the amount of fiber contents the slump value and the air content value shows similar results. Slump value was similar to 22cm, while the air content test results were about 3.4% (**Fig 4-2 (a)-(b)**). Special curing method for UHPC was necessary. The early curing after placing needs to maintain the high temperature and humidity for hardening. The slabs were covered with plastic and then subjected to an initial cure for one day as recommended in specification (**Fig 4-2 (c)**). After initial curing, high-temperature steam curing method was implemented for three days at a later day to exhibit fast strength development. High temperature wet curing was performed at $100°C$. In case that high temperature wet curing method is not performed well, the satisfaction of the performances of K-UHPC could be verified in advance. This curing method was demonstrated in K-UHPC code to provide improved tensile strength. Unlike the other concrete experiment, the tension test is considered importantly for confirming material performance. The tension test was conducted as stated in K-UHPC code.

The test specimens were constructed as shown in **Fig 4-2 (d)**.

After curing, the slabs were removed from the forms. All of the slabs exhibited a smooth surface on all sides that were in contact with the formwork, but the surfaces in the air were rough to the touch. A number of the slabs were poured in excess of the required thickness due to the lack of precision, but were deemed acceptable for testing. In addition, the two rows of bold holes were not placed exactly due to error in formwork fabrication or in the process of pouring UHPC. It required modifications to the frame and bolts, but it was also deemed acceptable for testing.

4.1.2 Compression Test

The improvement in compressive strength is the one of the most significant benefits of UHPC. In this paper, four types of K-UHPC with different fiber volume ratio were tested. For each type of K-UHPC, three specimens were tested. The results are as shown in **Table 4-2**. More fiber reinforcement causes larger compressive strength, but the gap in compressive strength is small enough to ignore. The maximum strain is about 0.002 for K-UHPC except for the 1.0% fiber-reinforced K-UHPC that has the maximum strain about 0.003. It seems that the maximum strain of K-UHPC is similar with the one of conventional concrete.

Table 4-2. Compressive Test Results

Fiber volume ratio	0%	0.5%	1.0%	1.5%
Compressive strength [MPa]	114.12	120.87	124.24	126.6
Maximum strain [μm/mm]	1974.9	1789.34	3075.9	1933.0

4.1.3 Tension Test

In this paper, four types of K-UHPC with different fiber volume ratio were tested. For each type of K-UHPC, three pieces were tested and the results are in **Table 4-3**. The ultimate tensile stress, f_{tk} was increasing while the fiber volume ratio was increased, but the tensile stress gap between 1.0% fiber-reinforced UHPC and 1.5% was very small. Additional, the standard deviation of ultimate tensile strength ($\sigma(f_{tk})$) was increased with the fiber volume ratio. The error in 1.5% K-UHPC tensile strength was 2.65 times bigger than the one in 1.0%. To get stable tensile performance 1.0% fiber reinforcement is better than 1.5%. More experiment is needed to find the most economic and reasonable fiber volume ratio that has good tensile performance even with the minimum fiber reinforcement.

The tensile behavior has only 10% performance of the compressive behavior in normal concrete, so the elastic limit in tensile stress was assumed to 10% of the 3000[μm/mm]. In this reason, the cracking stress, f_{crk} was measured when the strain was 300[μm/mm]. The ratio of cracking stress to ultimate tensile stress (f_{crk} / f_{tk}) was about 0.9, with more tests for understanding the tensile behavior the simple term ($f_{crk} = 0.9 \cdot f_{tk}$) will be able to adopted in code equation.

All of the K-UHPC test specimens except for the UHPC without fiber have almost same crack width when the tensile strength reached to the ultimate state. Regardless of the fiber volume ratio or the tensile strength, w_u and $w_{\lim}$ were almost same as shown in **Fig 4-3**. The previous tests and code (AFGC-SETRA) assumes that 0.3mm is the limit crack width for safety of the tensile strength. In this experiment the crack width at f_{tk} was bigger than 0.3mm, so the assumption can be adopted also in this paper.

Table 4-3. Tensile Test Results

Fiber volume ratio	0%	0.5%	1.0%	1.5%
Cracking stress, f_{crk} [MPa]	-	5.79	12.30	13.73
Ultimate tensile stress, f_{tk} [MPa]	4.07	6.43	14.98	15.12
Crack width at f_{tk}, w_u [mm]	0	0.54	0.4	0.44
Limit on crack width, $w_{\lim}$ [MPa]	7.53	6.95	7.12	8.2
w_u / $w_{\lim}$ [mm/mm]	0.0	0.077	0.056	0.053
Standard deviation for tensile stress, $\sigma(f_{tk})$	0.065	0.799	1.795	4.758

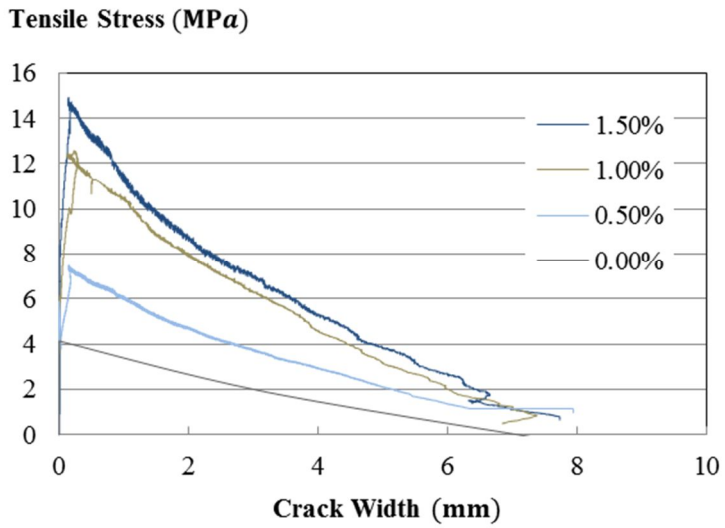

Fig 4-3. Crack width - Tensile stress Relationship for K-UHPC

4.2 Test Setting

4.2.1 Specimen Fabrication

In this paper, seven flat plate slabs are tested to get the punching shear strength and the behavior and the deformation during the failure. Specimens are designed as $1{,}600\text{mm} \times 1{,}600\text{mm}$ square shape slabs, and the clear span of the specimens excluded the length for the boundary is 1,200mm in each side (**Fig 4-4**). The thickness of the slabs are varies from 30mm to 60mm.

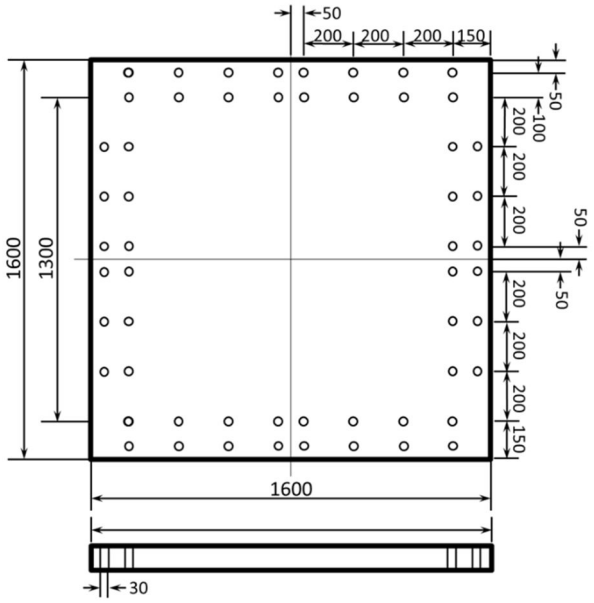

Fig 4-4 Test Specimen Black-out (up) and the Elevation (down)

4.2.2 Boundary Condition

Historically concrete slabs have been tested as simply supported systems loaded from above. Forming fully restrained slab systems gets into difficulty in design. In this paper, the objective of the experiment is observing the punching shear failure behavior. However, the thin UHPC

slabs tend to have the flexural failure behavior, and simply supported slab can have decrease in load due to flexural behavior. To achieve a punching shear failure, four sides of the specimens should be fully restrained. To embody the fully fixed boundary condition, the experimental jig that Dr. Joh (2011) designed for his UHPC slab test was employed. The jig has the bolts holes in two rows to prevent deflection of rotation of the edges. As shown in **Fig 4-5**, the slabs were supported by $H500\times200$ beams bolted to the reaction floor. The rotations and deflections of the slabs were restrained by $C200\times90$ channel sections on the top of the slab bolted through the slab and the supporting bean flanges.

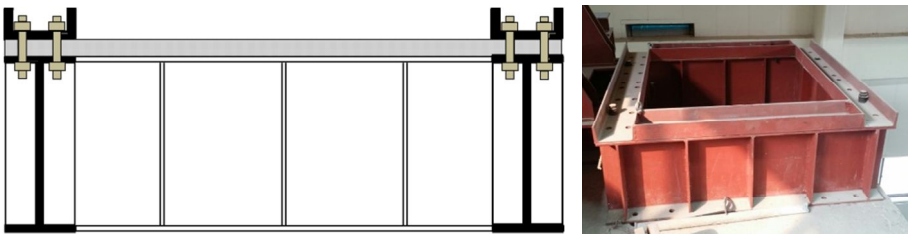

Fig 4-5 Fully restrained boundary condition

4.3 Specimen Plan

The variables for this experiment are the thickness of the slabs and the fiber volume ratio. The main data for the test is shown in **Table 4-4**. Specimens 1-4 are for comparing the punching shear behavior according to thickness. The influence of the fiber volume ratio can be read off by comparing specimen 2 and specimens 5-7

UHPC is characterized for the thin elements due to its high strength and the good stiffness, and it can be used to strengthen the slab by coating on the original slab. So, thin slab thickness from 30mm to 60mm is chosen to be tested. UHPC material tests with variety of fiber volume ratio have already done by several researchers, and they got the results

that the UHPC with more than 2% of fiber volume ratio does not have better effect than the lower one, and it can be even worse. To concentrate on the best performance and the economic design of the UHPC flat slab, the UHPC slabs with 0% to 1.5% of the fiber volume ratio are tested.

Table 4-4. Punching Shear Test Specimens

Specimen Number	Specimen Name	t	ρ_f
1	D30-f1.5	30	1.5
2	D40-f1.5	40	1.5
3	D50-f1.5	50	1.5
4	D60-f1.5	60	1.5
5	D40-f1.0	40	1.0
6	D40-f0.5	40	0.5
7	D40-f0.0	40	0.0

4.4 Experimental Setup

4.4.1 Frame

On UHPC thin plate characteristic, flexural failure can occur easily with large loading area. The punching area should be small as a projection of the wheel load on the slab. The loading area is $50\text{mm} \times 50\text{mm}$ expecting the punching shear failure. The size of the loading area was determined considering the results of the previous tests. To avoid the rotation of the slab, the loading was performed at the center (**Fig 4-6**).

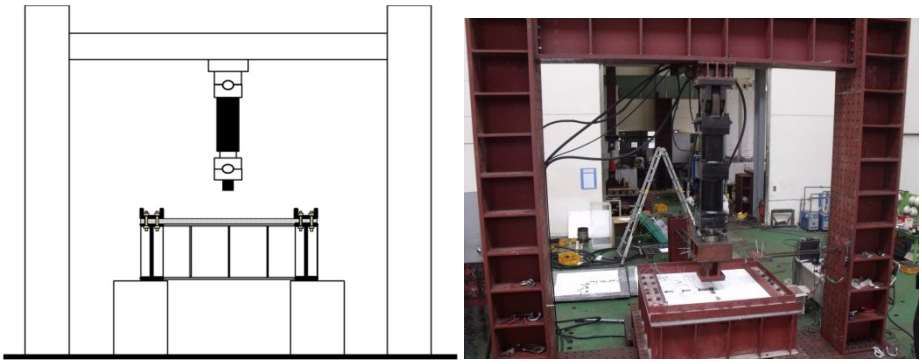

Fig 4-6 Jig setting

4.4.2 Loading

The slabs were loaded by 500kN actuator, and the loading rate was controlled in the displacement control method. Loading was applied in 0.03mm/sec of displacement increments. For the punching shear failures, the loading was continued until the slab was totally destroyed. The slabs were loaded until a decrease in load was observed in the load-deflection curve following the peak load.

The loading forces when it sounds like the slab has initial crack and the critical crack were recorded to determine the cracking behavior on the punching shear failure in slabs.

4.4.3 Measurement Plan

Measuring and observing deformations are very important to investigate the punching shear failure behavior of the slab. The vertical deflection, crack width, crack patterns and etc. were significantly considered in this paper.

The vertical deflection was measured by nine LVDT at the center of the loading, and 100mm, 200mm, 300mm, 500mm away from the loading pad. The measured vertical deflection can be used to determine the slab rotation that is crucial for defining the punching shear failure behavior (**Fig Fig 4-7 (a)**).

Four crack gauges are also equipped on the tension side (bottom of the slab) in parallel direction to the boundary and in diagonal direction. The crack gauges can determine the location of the critical crack and the crack pattern (**Fig 4-7 (b)**).

The concrete gauges are installed both on the tension side and the compression side to assume the strut angle that connects the crack on the compression side to the one on the tension side. On both sides twelve concrete gauges were used in two direction, right next to the loading pad, and 200mm, 400mm far from the loading pad. The location of critical part of the slab can be supposed by measuring the micro crack using concrete gauges (**Fig 4-7 (c)**).

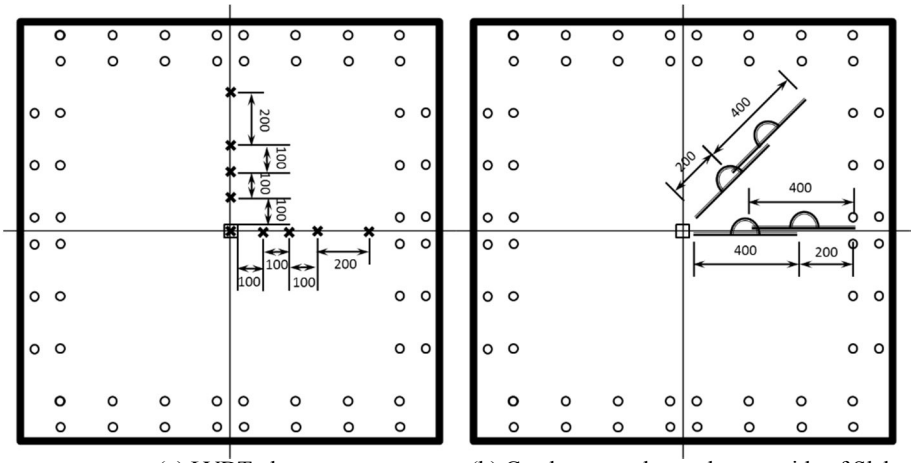

(a) LVDT plan (b) Crack gauge plan on bottom side of Slab

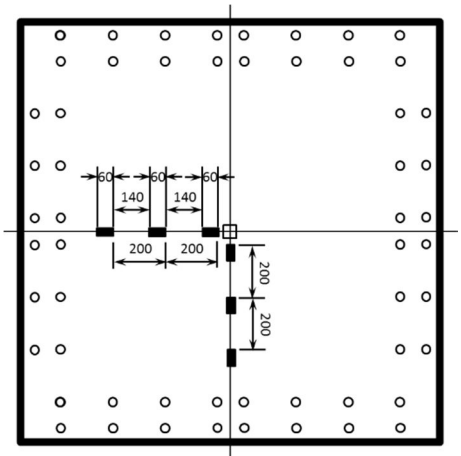

(c) Concrete gauge plan on top and bottom side of the slab

Fig 4-7 Measurement Plans on top and bottom side of the slab

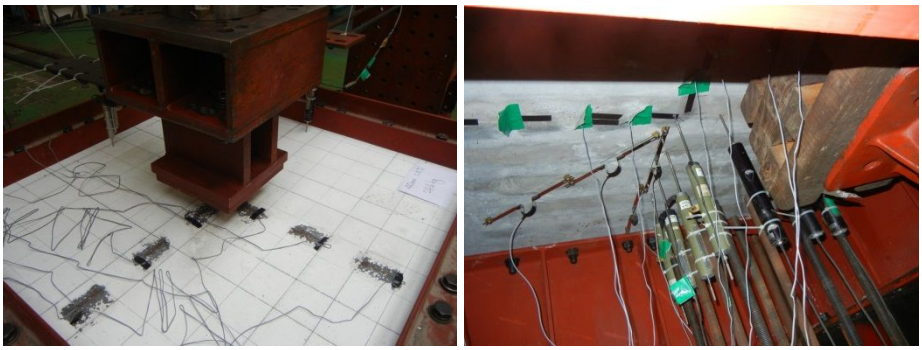

Fig 4-8. Photo of Measurement Plan (Top :Left, Bottom : Right)

Fig 4-8 shows the measurement plan on the bottom side of the slab. As shown in this figure, the concrete gauges, LVDTs (The linear variable differential transformer) and the crack gauges are installed on the tension side of the slab. The concrete gauges were also installed at the same places on the opposite side of the slab.

Chapter 5. Test Results and Analysis

5.1 Summary of the objectives of this experiment

In this paper, the measurement of deformation was essential to understand the punching shear failure mechanism. The vertical displacements varying with the distance were checked to find the location of failure section. The location of micro crack and the crack width were realized by the concrete gauge. The concrete gauges were applied at the same place on the top and bottom side, so that the strut angle that connects the tangential crack can be assumed. The crack gauges were installed to find out the distribution and the width of the critical cracks after the initial crack.

5.2 Failure Mechanism

5.2.1 General

By comparing the slabs made from UHPC and the conventional concrete (**Fig 5-1**) that are failed because of punching shear, the UHPC slab has shown more micro-cracks than the conventional concrete slab has . In **Fig 5-5,** the flat stage after the linear increase of punching load means the softening behavior. This softening stage is formed, because the micro cracks occurred on the UHPC slab allow that the slab can resist the punching load. When the cracks developed to the macro cracks, the slab failed. The reason that the micro cracks occur more on the UHPC slabs than on the conventional concrete is supposed the bridge formation of the fibers, and the tensile strength due to the bridge effect is the most important difference between conventional concrete and UHPC. Bridge phenomenon of the fibers in the UHPC allows the increment punching strength even after the micro cracks occur. When the punching load is about 10kN, there was small noise that sounds like the pull-out of

the fibers occur. After the punching load increases 70% of the ultimate punching shear strength, it sounds loudly like the fibers are ruptured.

In the Previous paper the conventional concrete slabs tend to have the failure section three to four times of depth far from the loading pad. In case of the UHPC flat plate, the main punching crack was occurred five to six times of depth far from the loading pad. The failure section of UHPC flat plate is larger than the one of original concrete, and it can mean that the UHPC slab has gentle strut angle smaller than 45°.

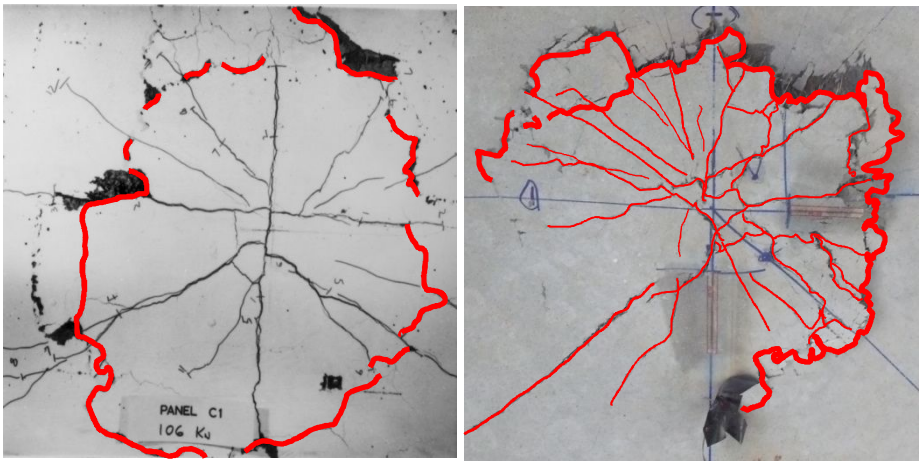

Fig 5-1. Punching Shear Failure Pattern of
(Normal Concrete Slab : Left, K-UHPC : Right)

Another characteristic of the UHPC slab is high punching shear strength. If the slab was made of conventional concrete, the large amount of steel is needed for stirrup. For example, the 30mm RC slab needs D10 stirrup every 15mm, the 60mm RC slab needs D16 stirrup every 30mm. Since the regulation of the minimum space for the stirrups is 100mm. This reinforcement design is inappropriate for practical structure. For thin plate or slab reinforcement, the UHPC will show the outstanding performance.

5.2.2 Punching Shear Strength and Displacement

The ultimate punching shear strength and the displacement at the ultimate load are like as follows in **Table 5-1. Fig 5-2** is the graph to find how the slab thickness affects to the punching shear strength and the deflection. The influence of the fiber volume ratio can be read off through **Fig 5-3.**

Fig 5-2 and **Fig 5-3** shows the relationship between the ultimate punching shear strength (V_u) and the maximum deflection ($\delta_{\max}$). In **Fig 5-2**, thicker slab could resist to higher punching strength, and the ultimate punching shear strength was inversely proportional to the deflection. This means that the thickness of the slab allows the increment of punching shear strength, and the decrement of the stiffness.

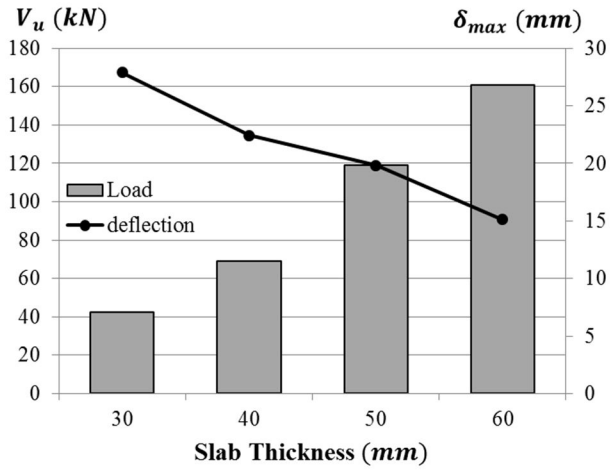

Fig 5-2. Ultimate Punching Shear Strength and Maximum Deflection Corresponding to the Slab Thickness

Increase in punching shear strength due to more fiber reinforcement leads to the Increase in the maximum displacement, as shown in **Fig 5-3**. For 0% to 1% of fiber volume ratio, the higher fiber volume ratio means that strength and stiffness are getting higher and better. However, the slabs reinforced by 1% of fibers and 1.5% of fibers were not that different and the 1%-fiber-reinforced slab has shown even better strength and stiffness. The previous material tests found that excessive amount of

reinforcing fibers disturb to be distributed evenly. So the strength of the UHPC is rather be lesser than the one with lesser reinforced. From this, the study to find out the proper and economic fiber volume ratio that has the best performance should be done in further research

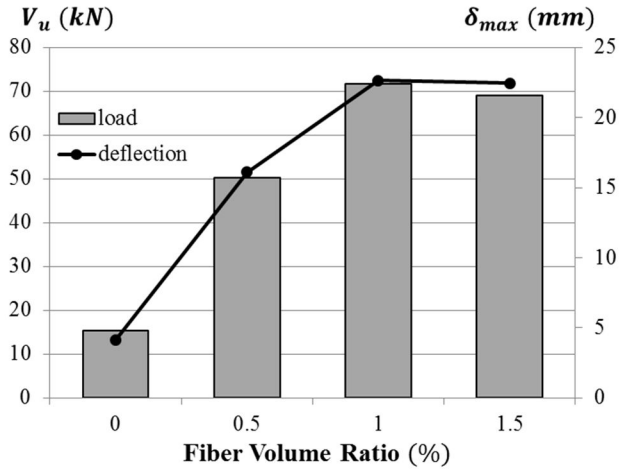

Fig 5-3. Ultimate Punching Shear Strength and Deflection Corresponding to the Fiber Volume Ratio

Table 5-1 Punching Shear Test Results

Specimen Number	Specimen Name	Maximum deflection δ_{max}[mm]	Ultimate Punching Shear Strength V_u[kN]
1	D30-f1.5	27.90	42.19
2	D40-f1.5	22..44	69.05
3	D50-f1.5	19.81	118.94
4	D60-f1.5	15.12	160.80
5	D40-f1.0	22.65	71.65
6	D40-f0.5	16.1	50.33
7	D40-f0.0	4.13	15.43

5.2.3 Relationship between the tensile strength and the punching shear strength

The existing formulas have different tensile strength terms. The split cylinder strength is adopted in Narayanan's equation. It is calculated from the equation as follow, $f_{spf} = \frac{f_{cu}}{20} + 0.7 + \sqrt{\frac{\rho_f d_f L}{D}}$. It considers the fiber effect, but mainly affected by the compressive strength of cube concrete. The influence of the fiber volume ratio is very smaller than the other tensile strength term. The JSCE code contains the design tensile strength term (f_{tk}), and the K-UHPC code contains the design average tensile strength in the direction perpendicular to the diagonal tensile crack (f_{vd}). As shown in **Fig 5-4**, the average tensile strength, f_{vd} is the most proportional term with the punching shear strength. While the equations have simple form that multiplies the coefficients to the tensile strength term, the feasibility of tensile strength term and punching shear strength is considered importantly. The direct tensile term has the uneven curve. It is considered that the direct tensile strength is not suitable to be applied for estimating the punching shear strength. The un-unified crack width is assumed for the reason of un-proportional relationship between the direct tensile strength and punching shear strength. The direct tension test specimens have perpendicular crack to the loading direction. However, the slabs have cracks in several ways. Therefore, the application of average tensile strength that considers the tensile strength according to the crack width is proper. Also, the directivity of the fibers could be another reason. While it is easy to control the fibers to be arranged in a row in a small direct tension test specimens, but the fibers in the slab does not have specific directivity.

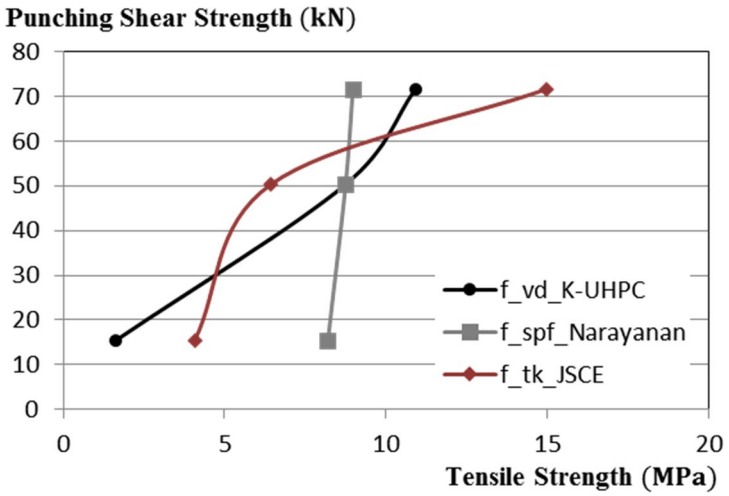

Fig 5-4 Relationship between the Tensile Strength Term and the Punching Shear Strength

5.2.4 Relationship between the load and deflection

The relationship between the load and deflection is presented to the graph corresponding to the thickness of the slab (**Fig 5-5**) and the fiber volume ratio (**Fig 5-6**). Different with the conventional concrete slab that fails in brittle manner, the UHPC slabs can keep resisting the punching load with more displacements after the slabs reached the ultimate load. The graph shows uneven curve. Increasing part due to the lengthened fiber maintaining the tensile strength, and the decreasing part due to the failure of fiber are repeated in small section.

Thin slab tends to resist more with longer softening stage. It is considered that the thinner slab is affected more by the flexural behavior. For the 40mm thickness slabs with different fiber volume ratio except for 0%-reinforced-slab, the more fibers lead the more punching shear strength and the higher stiffness.

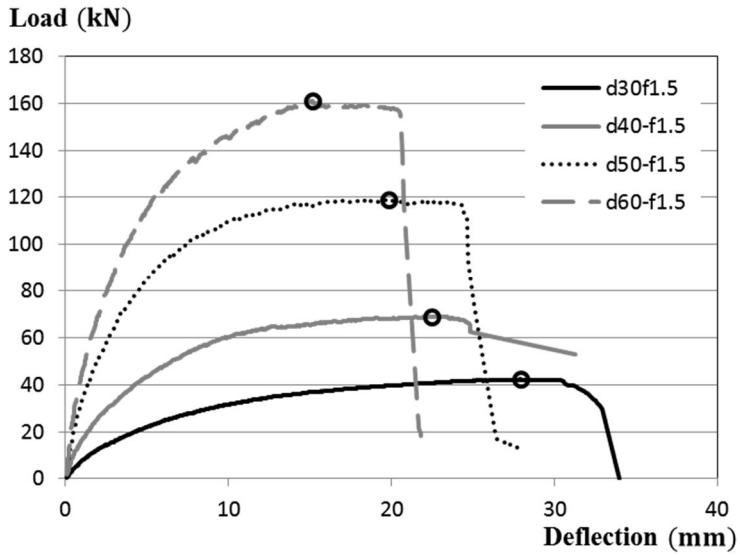

Fig 5-5. Load-deflection relations corresponding to the thickness of the slab

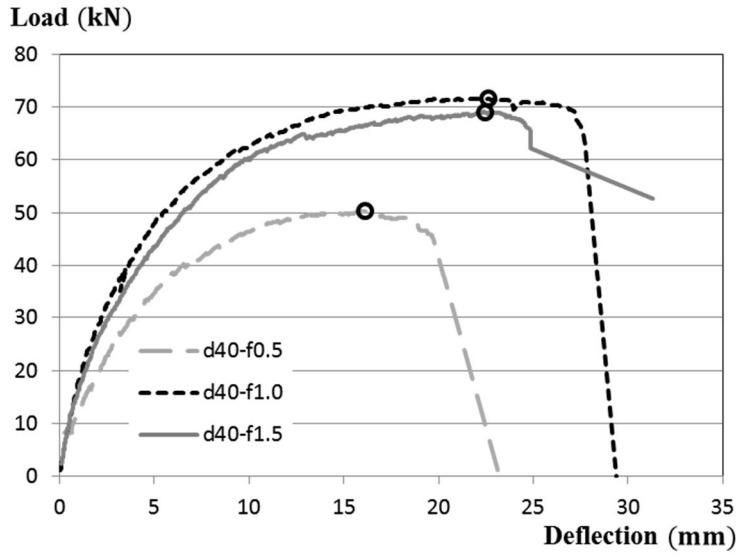

Fig 5-6. Load-deflection relations corresponding to the fiber volume ratio

5.3 Failure Behavior

The establishment of the most economical and safe standard that can estimates the punching shear strength of thin UHPC slabs is the final goal. For the proper development of punching strength calculation formula, identification of the failure behavior is very important. For this reason, the observation of the displacements was considered as the one of the most important task in this paper.

By comparing the strain behavior of each slab, the failure type and the critical parts can be predicted. The concrete gauges are installed both on the tension side and the compression side to assume the gap of the strain on the opposite side in same part. On both sides twelve concrete gauges were used in two directions. The gauges right next to the loading pad are series 1, the gauges 200mm apart from the loading pad are series 2, and the gauges 400mm far from the loading pad are series 3. The attached letter 'T' in the front means the top of the slab (compressive side), and 'B' means the bottom of the slab (tension side). The location of critical part in the slab can be supposed by measuring the most deformed part.

The strain response of the gauges on the loading face was different as a result of gauges being in compression throughout the testing. The strains recorded from the mounted strain gauges were assumed highly dependent on the crack pattern. The fibers prevent the crack from being wider, micro-crack to macro-crack. This effect of fibers leads to the significant performance as a stress distributor. Prevention of the macro-crack formation caused more micro-cracks. The micro-cracks spread on the wider part, and it distributes the stress. Therefore, with the better fiber effect the micro-crack is expected to be spread.

5.3.1 Strain Distribution according to the fiber volume ratio

The brittle failure of the slab without fibers (Specimen 7) caused the uneven line on the displacement graph. Without any reinforcement the concrete could not get the tensile strength effectively, and the failure was occurred in an instant. By comparing the results of Specimen 7 with

the results of other slabs reinforced by fibers, it is certain that the most important role of fibers were performed well. The fiber reinforcement allows the UHPC slabs to fail in a ductile manner accompanying increments in punching shear strength. By comparing the strain behavior of each slab, the critical parts can be deduced. With the result, the failure type can be predicted.

(a) Specimen 6 (40mm -0.5%) Strain Distribution

The compression was shown as a negative value. As shown in **Fig 5-7**, the strain values on the gauges located near the loading pad have the opposite sign with the strain values from the further gauges. It leads to the result that the limit to the critical area for punching shear failure on the compression side can be defined up to the distance of 110mm. The specimen 6 reinforced by 0.5% of the fibers tends to have wide crack near the boundary part. The strain values of series 3 –concrete gauges are larger than the strain values of the other gauges. Series 3 –gauge values are rapidly increased near the ultimate punching load. The macro-crack was occurred near the boundary part. The perfect reason for this whether it is due to the effect of the boundary condition or the flexural failure is not certainly approved. This specimen shows more brittle failure behavior than the other specimens, so the failure on the boundary part can be insisted with more possibility. For identifying this reason, the experiments on lower fiber volume ratio slabs and observation of failure behavior are essential in further study.

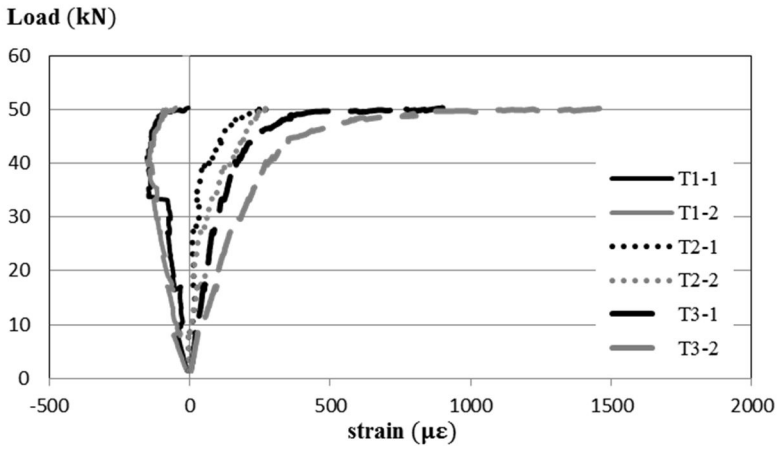

Fig 5-7 Typical Load vs. Strain (Top) for Specimen 6

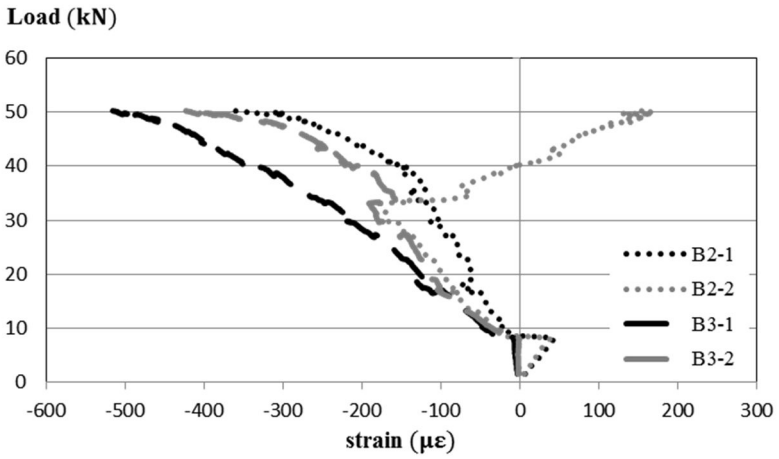

Fig 5-8 Typical Load vs. Strain (Bottom) for Specimen 6

The strain values on the gauges located on the tension side of the slab show the rough graph (**Fig 5-8**). Series 1 –gauges could not work and the one of series 2 –gauges shows a relieved line that implies the failed crack on that part. It was just assumed that there were wide crack right after the loading. Same with the graph on the top side of the slab, the boundary part seems the most critical part.

(b) Specimen 5 (40mm -1.0%) Strain Distribution

As shown in **Fig 5-9**, the strain values on the gauges located near the loading pad have the largest maximum value. The specimen 5 reinforced by 1.0% of the fibers tends to have wide crack near the loading area part. Series1 –gauge increases proportional to load increases until failure, after which the compressive strain is relieved as the loading area pulled out through the plate. The cracks were not extended wider near the boundary part. The deformation behavior was concentrated near the punching area. From this, it can be predicted that this specimen has the failure behavior that is close to the pull-out punching shape.

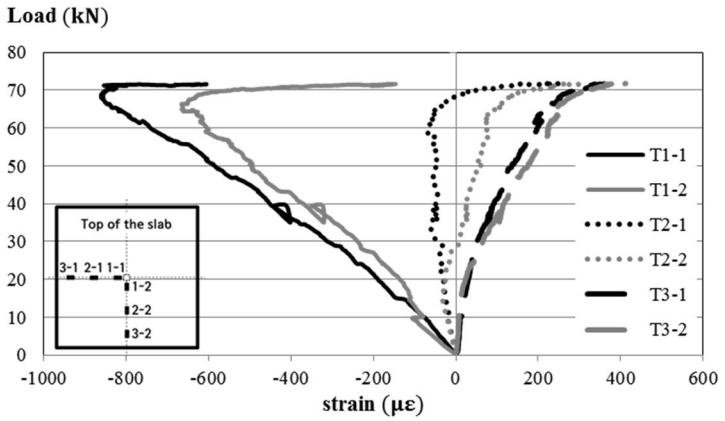

Fig 5-9 Typical Load vs. Strain (Top) for Specimen 5

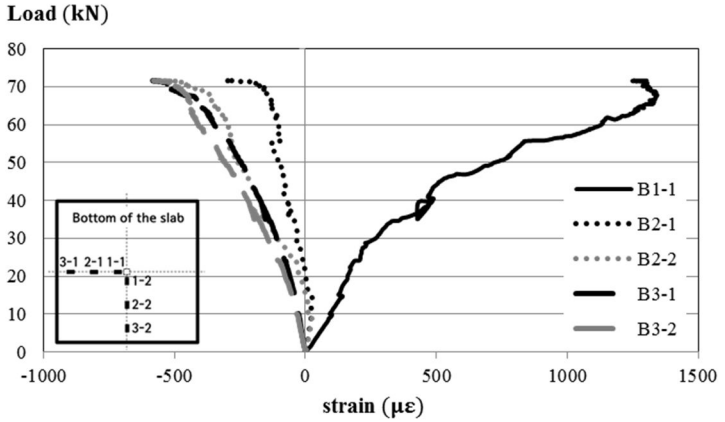

Fig 5-10 Typical Load vs. Strain (Bottom) for Specimen 5

The strain values on the gauges located on the tension side of the slab were illustrated in **Fig 5-10**. One of series 1 –gauges could not work, and the other one shows an uneven line. It was just assumed that this part has large deformation during the loading. This critical part is appeared by concentrating the punching load. The fibers performed on the part that has the micro-crack to prevent from the macro-crack formation. While more fibers yield, the increment on strain is getting faster. This part can be defined as the critical area for the punching shear. Same with the graph on the top side of the slab, near the loading part seems the most critical part.

(c) Specimen 2 (40mm -1.5%) Strain Distribution

As shown in **Fig 5-11**, the strain values on the gauges located near the loading pad and one of the series 3 –gauges show large maximum value before relief. The specimen 2 reinforced by 1.5% of the fibers tends to have both punching shear failure and flexural failure behavior. T1-2 gauge increases proportional to load increases until failure. The increment of T3-1 gauges was larger near the failure. After the loading area was pulled out, the compressive strain is relieved. There was another critical part near the boundary jig. The deformation behavior was diffused as the central figure from the punching area. However, the cause of the wide crack formation near the boundary is not clear yet. By observing the failure pattern of the slab visually, narrow cracks were occurred near the bolt connections. Whether it is just from stress contribution or the boundary effect should be clear up. To clear up this point, more studies that allow the observation of boundary deformation should be carried out. If the large deformation on the boundary part is neglected, it can be predicted that this specimen has the failure behavior that is close to the pull-out punching shape.

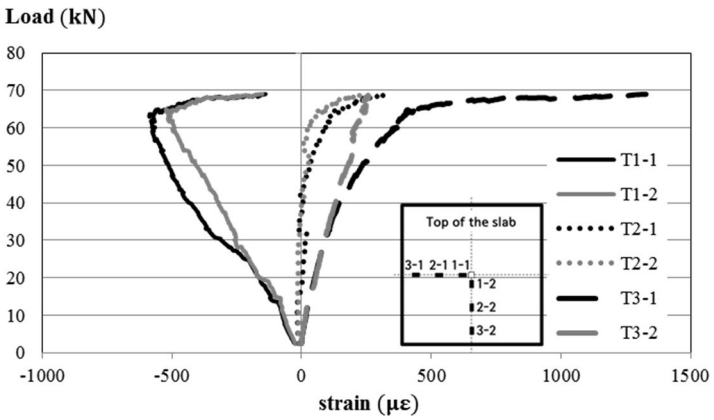

Fig 5-11 Typical Load vs. Strain (Top) for Specimen 2

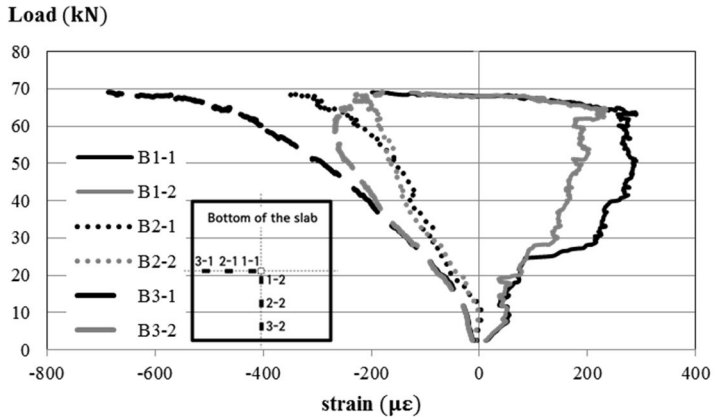

Fig 5-12 Typical Load vs. Strain (Bottom) for Specimen 2

The strain values on the gauges located on the tension side of the slab were illustrated in **Fig 5-12**. The series 1 –gauges show the uneven lines unlike the other gauges. It was just assumed that this part has large deformation during the loading, same with the specimen 5. When the loading is slightly over 25MPa, the strain values are increased rapidly in a while. This part can be explained as that many fibers on that critical area were yield simultaneously. Same with the graph on the top side of the slab, the increment of T3-1 gauge was very large near the failure. The deformation seems that is getting across to the opposite side of the slab.

(d) Comparison of Strain Distribution according to the fiber volume ratio

As shown in **Fig 5-13,** the strain distribution graphs according to the load were drawn. The strain distributions of three specimens with different fiber volume ratio were compared. The first series gauges on the compression side of the plate were considered as the most critical part, and these data were selected to be compared. Specimen 6 that was reinforced by 0.5% of fibers has shown the most brittle failure among three slabs. It shows not only the lowest punching load but also the smallest deformation capacity. The initial inclination of every gauge seemed almost similar. When the punching load was close to 10MPa, specimen 2 and 5 that are reinforced by 1.5% and 1.0% of fibers each shows increased inclination on strain values. Before the experiment was performed, the best deformation capacity and the punching load were expected for the specimen 2 that has the largest amount of fiber reinforcement. However, the specimen 5 with 1.0% of fiber reinforcement shows better deformation capacity. Even the ultimate punching shear strength value of specimen 5 was larger than the one of specimen 2. The previous material tests found that excessive amount of reinforcing fibers disturb to be distributed evenly. So the strength and the deformation capacity of the specimen 2 can rather be lesser than the one of specimen 5.

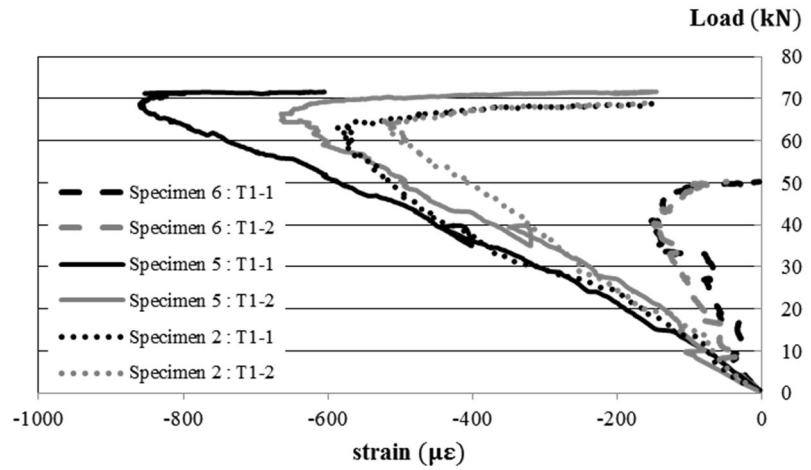

Fig 5-13 Typical Load vs. Strain (Top) according to the Fiber Volume Ratio

5.3.2 Strain Distribution according to the slab thickness

The expected failure behavior of test specimens was punching shear failure. The actual failure behavior even on this experiment has shown combined punching shear failure and flexural failure behavior. The small ratio of the thickness and the slab width is considered to affect the slab to fail in flexural behavior. Therefore, the failure behavior of thin plate should be carefully observed. It is hard to distinguish the punching shear failure from the flexural failure. The consideration of the failure behavior according to the slab thickness is necessary in the code for regulating the minimum thickness or the proper design method for thin slabs. In this paper, to arrange the proper data for the further study, the detail on failure behavior of the slabs was recorded.

If the slabs experienced the theoretically perfect punching shear failure behavior, the deformation would be occurred only at the punching area. In practical experiments, the slabs have both punching and flexural behaviors. To distinguish the two failure mechanisms, the deformation behavior should be carried out in detail. In this paper, the location of the gauge that has the most critical value was importantly treated to assume the position of the critical crack. The large deformation near the boundary part can be formed due to the flexural failure. From the concentrated deformation near the punching area, the punching failure can be expected.

(a) Specimen 1 (30mm -1.5%) Strain Distribution

The specimens experienced both flexural and punching shear failures. The strain response among the two failure mechanisms was observed to be similar in nature and dependent on the location of the strain gauge placement relative to the crack formation pattern. In both the flexural and punching shear failure, the predicted failure loads were higher than the actual failure loads. This trend is understandable for the flexural failures. The interpretation of this difference can likely be attributed to a failure mode different from the predicted failure behavior.

Specimen 1 has larger strain near the boundary as shown in **Fig 5-14** and **Fig 5-15**. This can lead to the point that the boundary part is

the most critical part in this specimen. The strain increment near the punching area is not significantly larger than the strain increments on the other part. Specimen 1 shows both punching shear failure and the flexural failure behavior, but the primary failure pattern was assumed as flexural behavior. With the flexural behavior on whole slab, the slab could not resist the punching load as much as predicted previously. To apply the effect of tendency of flexural failure on thin slabs, the regulation of the minimum thickness or the proper estimation formula for thin slab that considering the flexure should be prepared.

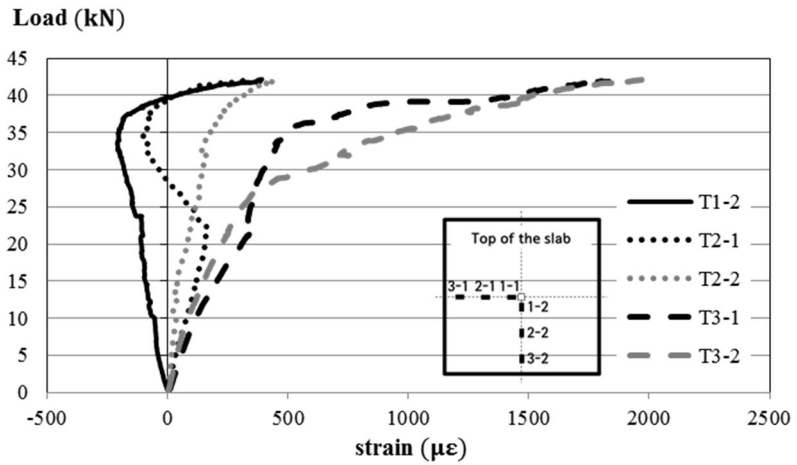

Fig 5-14 Typical Load vs. Strain (Top) for Specimen 1

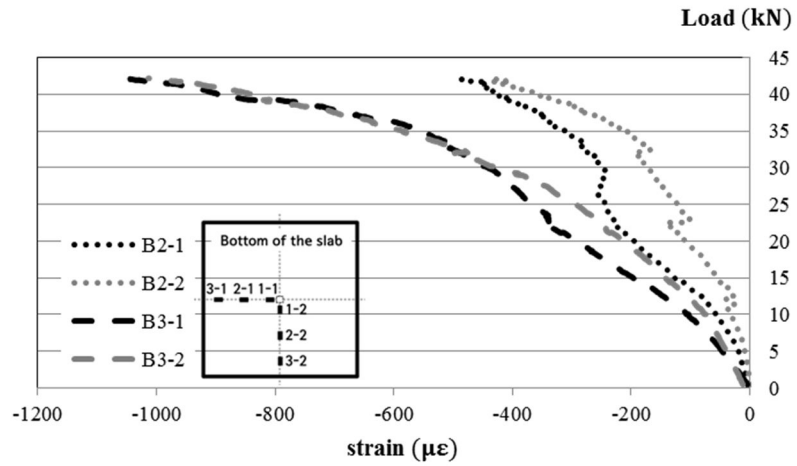

Fig 5-15 Typical Load vs. Strain (Bottom) for Specimen 1

(b) Specimen 2 (40mm -1.5%) Strain Distribution

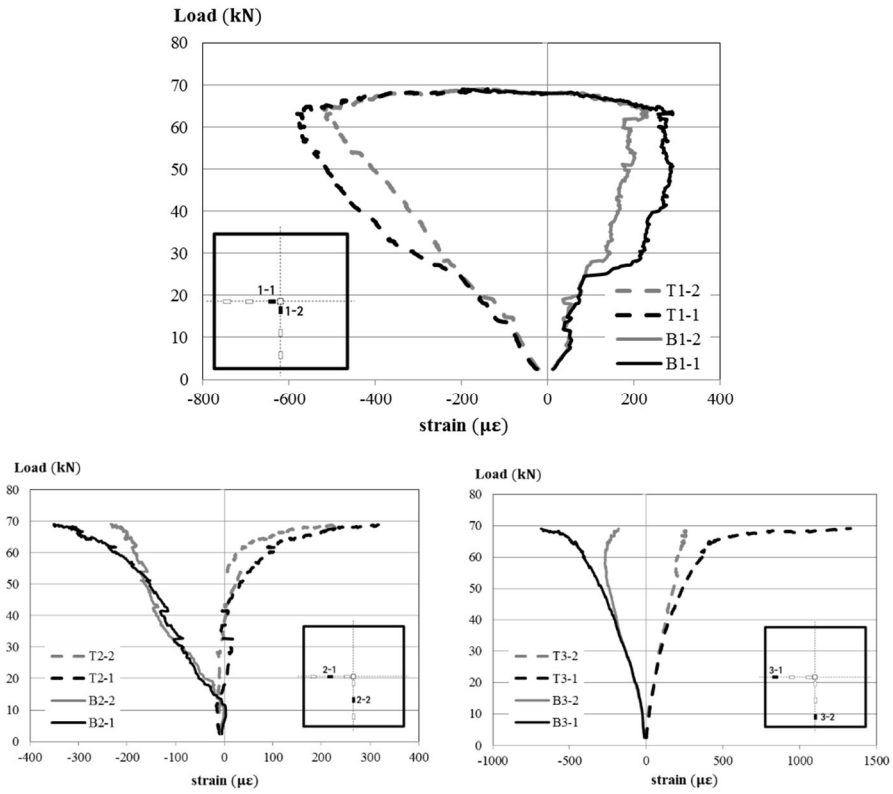

Fig 5-16 Typical Load vs. Strain (top and bottom) for Specimen 2

The strain gauge values on the top and bottom sides of the slabs are expected to show the connection of the crack, and to explain the strut angle that transforms the compressive strength to the opposite side of the slab. By comparing the inclination of the series 1 and 3 strain response, primary failure behavior can be supposed. The series 1 gauges show larger strain value on the compression side of the slab. It can be assumed that the transformation of the compressive strength that leads to the punching shear failure was not significant. On the other hand, the increment of the strain on series 3 shows the tension side has larger value. In the **Fig 5-11** illustrated previously, it shows the strain values on gauge series 3 are larger than on series 1. The diffused strain on the slabs represents the combined the failure behavior of flexure and punching

shear. However, the flexural failure behavior of the specimen 2 was not as significant as the one of specimen 1. This can be studied for defining the boundary of the punching shear failure and the flexural failure. By comparing the series 1 and 3 with series 2, the strain curve on the tension side shows more irregular near the loading area and boundary. This can stand for the fact that the location near the loading area and boundary are D-region that the critical failure occurs, and the location on the part of gauge series 2 are B-region that shows more ductile behavior.

(c) Specimen 3 (50mm -1.5%) Strain Distribution

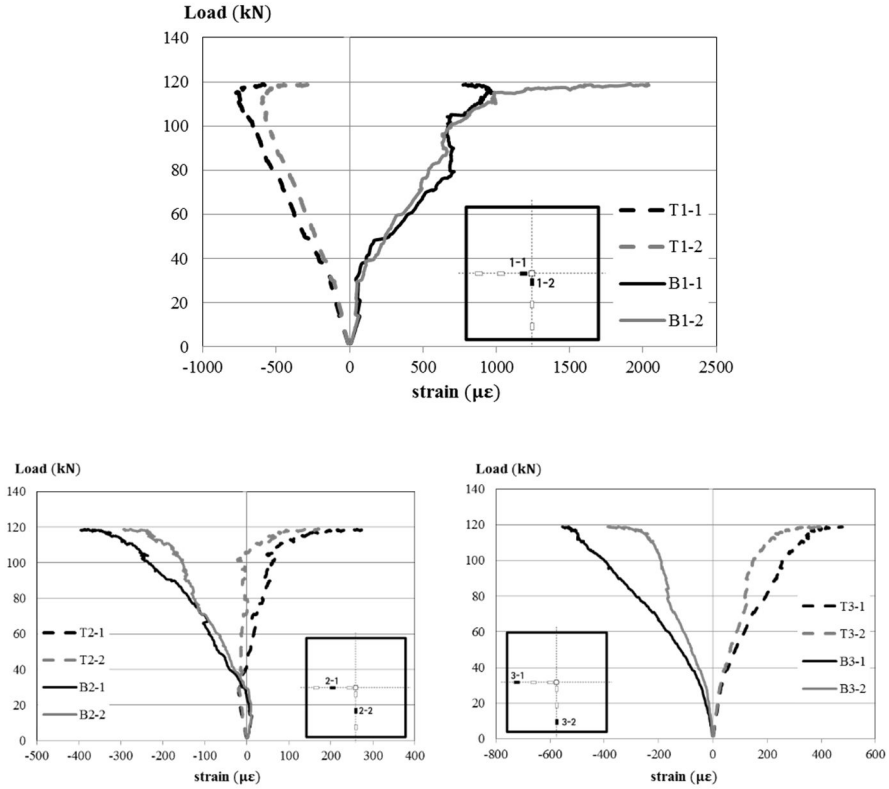

Fig 5-17 Typical Load vs. Strain (top and bottom) for Specimen 3

By comparing the strain gauge values on the top and bottom sides of the slabs, the connected relationship of the crack formation on the compression side and the tension side can be analyzed (**Fig 5-17**). The

strain response of the gauges on the loading face was different with the strain response of the ones on the tension face. The gauges on the tension side show irregular increments, while the other side gauges show more even increments. In general, the maximum strain on the tension side shows larger value than the one on the compression side.

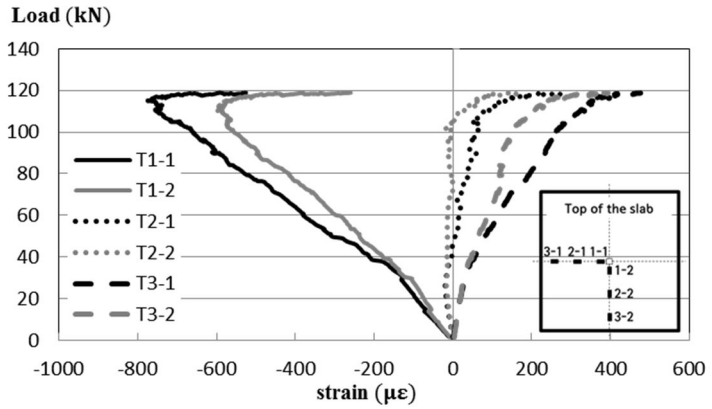

Fig 5-18 Typical Load vs. Strain (Top) for Specimen 3

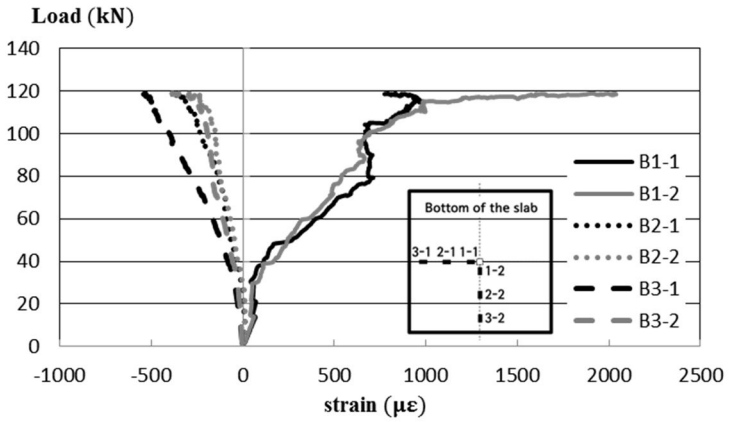

Fig 5-19 Typical Load vs. Strain (Bottom) for Specimen 3

The strain curve shown in **Fig 5-18** and **Fig 5-19** compares the strain values according to the location on specimen 3. The specimens are experienced both flexural and punching shear failures. Unlike the upper slabs, it shows the strain values on gauge series 1 are larger than other

gauges'. The concentrated strain near the punching load represents the failure behavior of punching shear. It could not be said that there is no flexural behavior in this slab. However, in specimen 3 the punching shear failure behavior was more significant than the flexural behavior.

(d) Specimen 4 (60mm -1.5%) Strain Distribution

The strain distribution on specimen 4 shows almost similar aspects with the specimen 3 (**Fig 5-20**). The gauges on the tension side show irregular increments. The strain response collected from the other side of gauge is almost proportional to the load until failure. Regardless of the location, the strain was larger on the tension side of the slab.

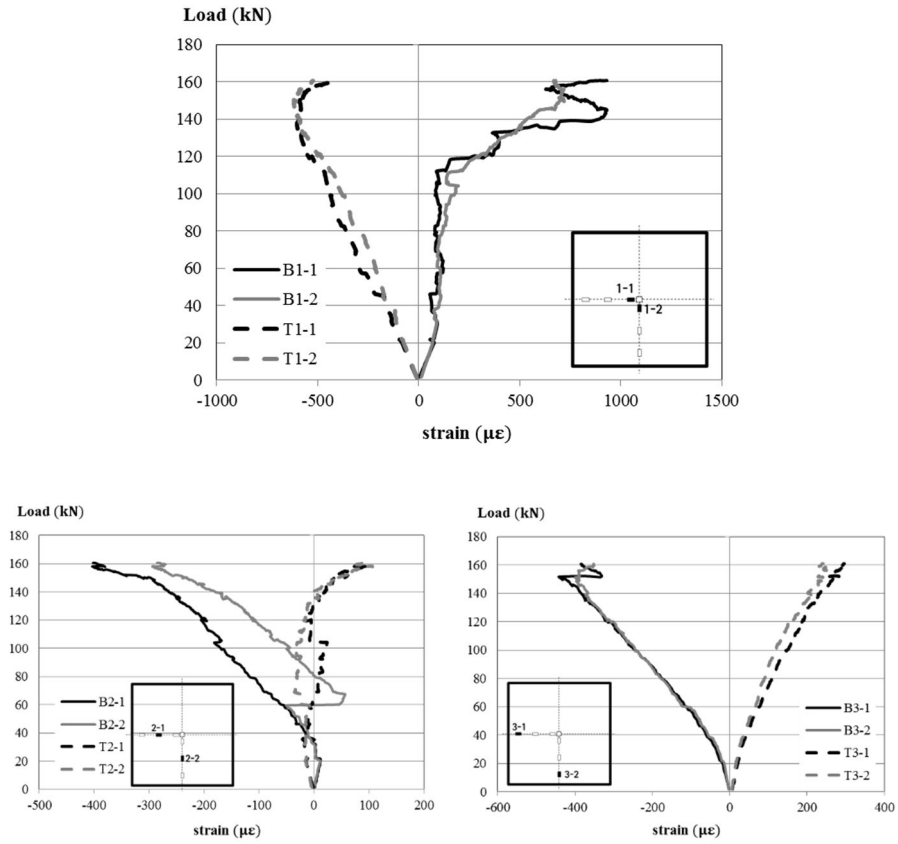

Fig 5-20 Typical Load vs. Strain (Top and Bottom) for Specimen 4

The most critical part on this slab can be assumed with the largest strain value, and the location is near the punching area on the bottom side. In this part, the tension failure will occur that causes the brittle failure of slab. The punching shear failure behavior of the slab is certain with the evidence of confirming that the most critical part is punching area.

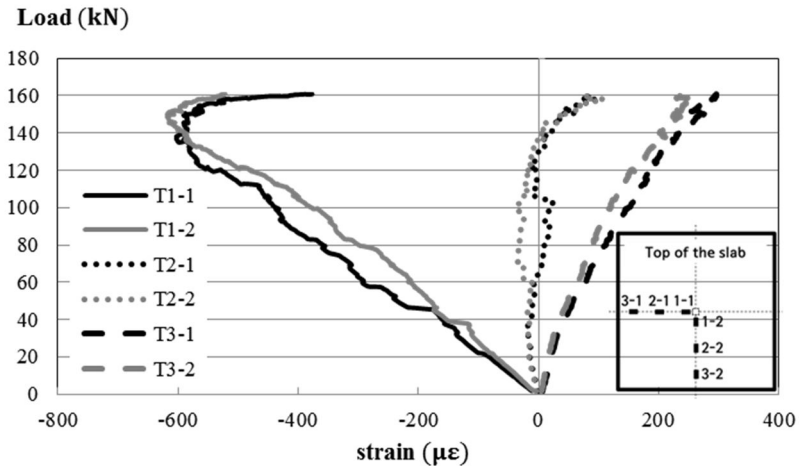

Fig 5-21 Typical Load vs. Strain (Top) for Specimen 4

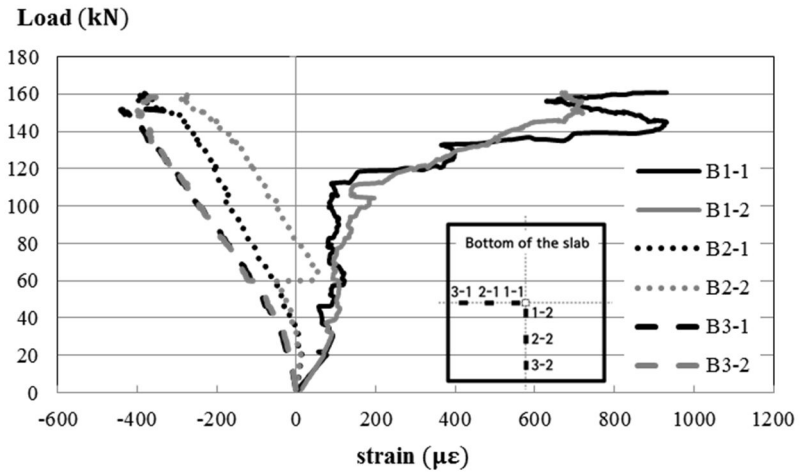

Fig 5-22 Typical Load vs. Strain (Bottom) for Specimen 4

(e) Comparison of the strain distribution according to the slab thickness

The strain distributions in accordance with the slab thickness were illustrated for comparing the effect of slab thickness. Series 1 and Series 3 on the compressive side of the slabs were importantly treated. **Fig 5-23** illustrated the strain values near the punching area (Series 1) will show the punching behavior. The strain response near the boundary (Series 3) is illustrated in **Fig 5-24**, and it will show that the specimens strongly affected by the flexural behavior.

As shown in **Fig 5-23**, the increment of the strain values is faster for the thinner slabs. Except for the slab with 30mm thickness, the inclination of strain was getting higher with the thicker slabs. The thicker slabs tend to be failed in brittle manner. Even though there was no big difference in deformation capacity between the slabs excepting slab with 30mm thickness, they have different stiffness. Therefore, the thicker slab could reach higher ultimate punching load.

For observation of the effect of flexural behavior on slabs, the deformation near the boundary (Series 3) should be carefully measured. As the flexural failure occurs, the deformation on the edge of the slab is getting larger. In this **Fig 5-24**, it shows same appearance with the above one that the inclination of the strain was getting higher with the thicker slabs. By comparing the pace that the strain reaches the peak point of punching load, the deformation capacity seems not that different. However, the final deformation in this place is getting larger for the thinner slabs. Especially, the ultimate strain value of slab with 30mm and 40mm thickness were significantly large. The macro-crack seems to be occurred in this part when the slab fails. The assumption that the flexure occurs on the edge of the slab can be adopted for this graph. For the strain values on 40mm-thick, the definition of the boundary for flexural failure and punching shear failure should be provided.

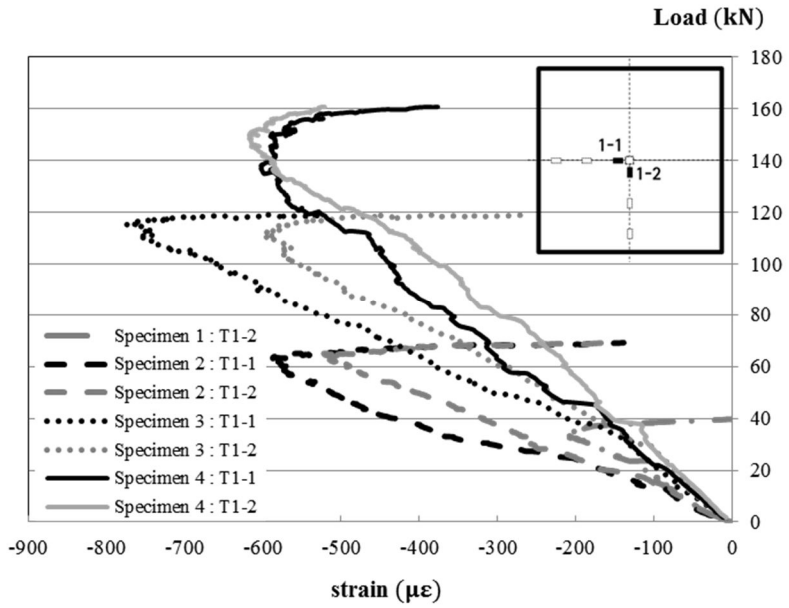

Fig 5-23 Typical Load vs. Strain (Top, Series 1) according to the Slab Thickness

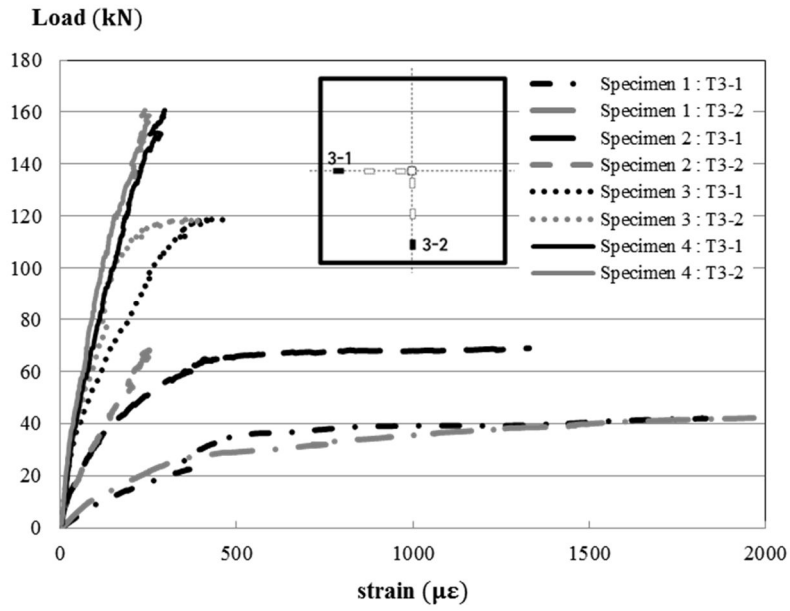

Fig 5-24 Typical Load vs. Strain (Top, Series 3) according to the Slab Thickness

5.3.3 Failure Section

A punching shear failure is typically a brittle failure that occurs with limited warning, and for the UHPC slabs this occurred when the slab failed to support additional load followed by a conical punching failure. The cracking was occurred in uneven directions. This led to the conclusion that the fibers could be randomly oriented. This phenomenon should be attributed to the casting technique. Pouring the UHPC in uniaxial direction with a trough system can result in alignment of the fibers parallel to the direction of pouring. This assumption is in agreement with the trend described by the AFGC recommendations (2002) in that the fibers tend to align with the direction of the pour and along the formwork.

(a) $d = 40mm, \rho_f = 0.0\%$ (Right after the loading : Left, After removal of jig : Right)

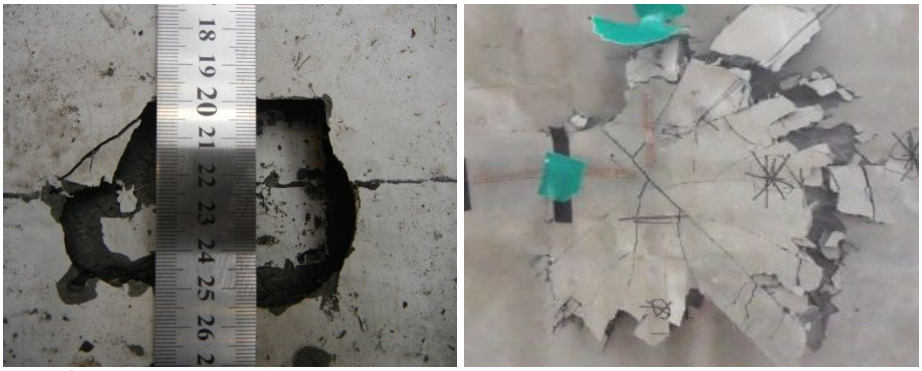

(b) $d = 40mm, \rho_f = 0.5\%$ (Compression side of slab : Left, Tension side of slab : Right)

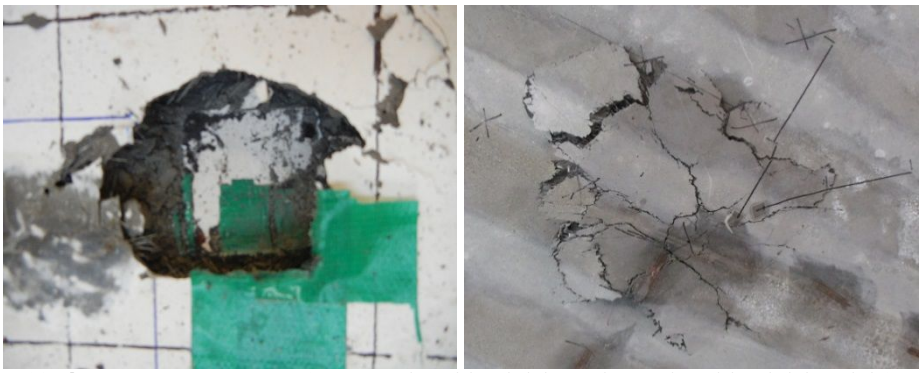

(c) d = 40mm, ρ_f = 1.0% (Compression side of slab : Left, Tension side of slab : Right)

Fig 5-25 Failure Pattern according to the Fiber Volume Ratio

The failure patterns according to the fiber volume ratio are shown in **Fig 5-25**. The compression side of the slab has similar crack pattern regardless of the fiber volume ratio or the slab thickness. On the top of the slab the cracked section was almost same with the loading area. The loading pad was almost stuck in the slab, and only some fragments were appeared near the loading area. By observing that the failure area on top side of slab is same, the critical section of the compression side can be assumed to the same area with the loading area.

The slabs with different fiber volume ratio have shown similar failure patterns, except for the unreinforced slab. Unreinforced UHPC slab has broken in a completely brittle manner. The crack pattern could not be found, and the maximum deflection was only 1/4 to 1/5 of the other slabs. The slabs with volume fiber ratio of 0.5% and 1.0% show almost $27,500mm^2$ of failure section. The punching area was formed as conical shape, and the pull-out failure could be defined.

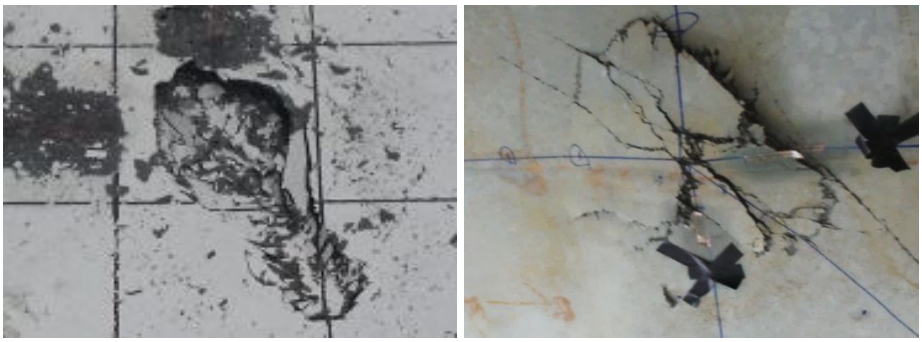

(a) d = 30mm, A_c = 29,750mm^2

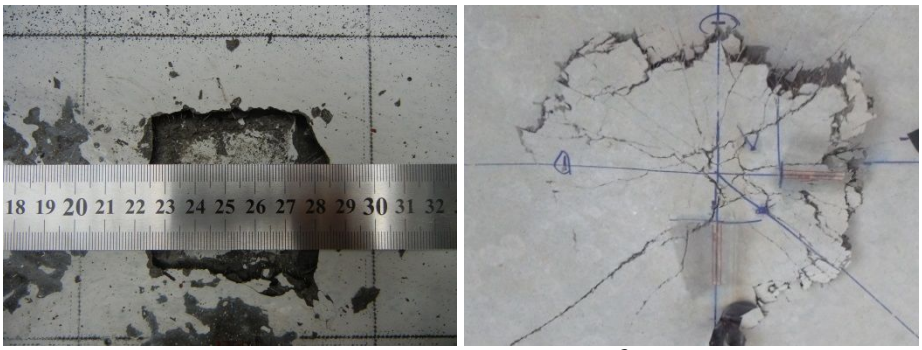

(b) d = 40mm, A_c = 27,500mm^2

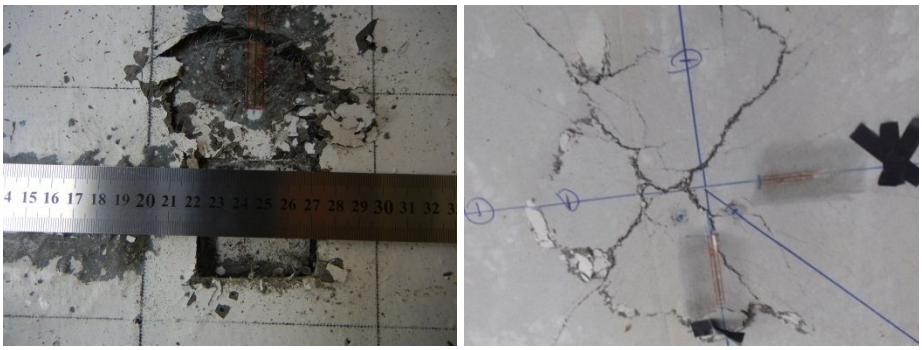

(c) d = 50mm, A_c = 41,900mm^2

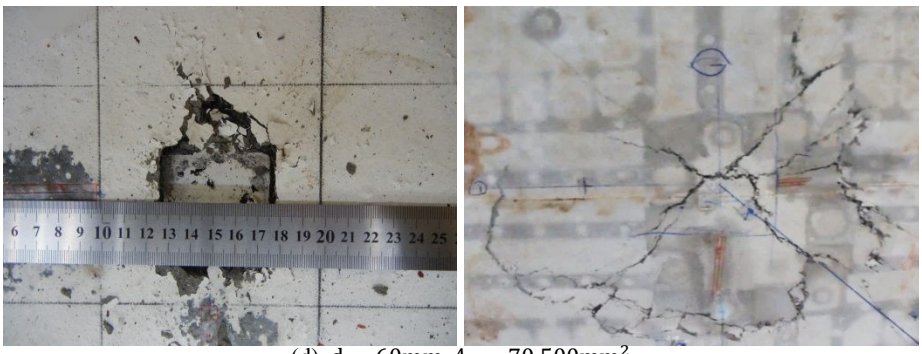

(d) d = 60mm, A_c = 70,500mm^2

Fig 5-26 Failure Pattern according to the Slab Thickness
(Compression side of slab : Left, Tension side of slab : Right)

The failure area according to the slab thickness has shown noticeable tendency as shown in **Fig 5-26**. Thicker slab shows larger failure area. However, the failure area of the slab with 30mm thickness shows 29,750mm^{2}little larger than one of the 40mm-thick slab. The failure pattern of 30mm-thickness slab was little different with the other slabs. It shows elongated failure area, and redeemed to be affected by the flexural failure behavior. The slabs tested failed at loads lower than predicted. The slabs have shown both flexural and punching shear failure aspects. The reasons of the overestimation of the punching shear strength are supposed to the effect of moment capacity and the degree of fixity at the supports. From these two conditions, the distinct feature that the UHPC slabs tend to have the flexural failure behavior can be assumed. The 30mm-thick slab is considered to be affected by the flexural behavior more than others. The guideline for the limit of the thin plates or the consideration of the flexural failure strength for thin slabs should be studied in further study.

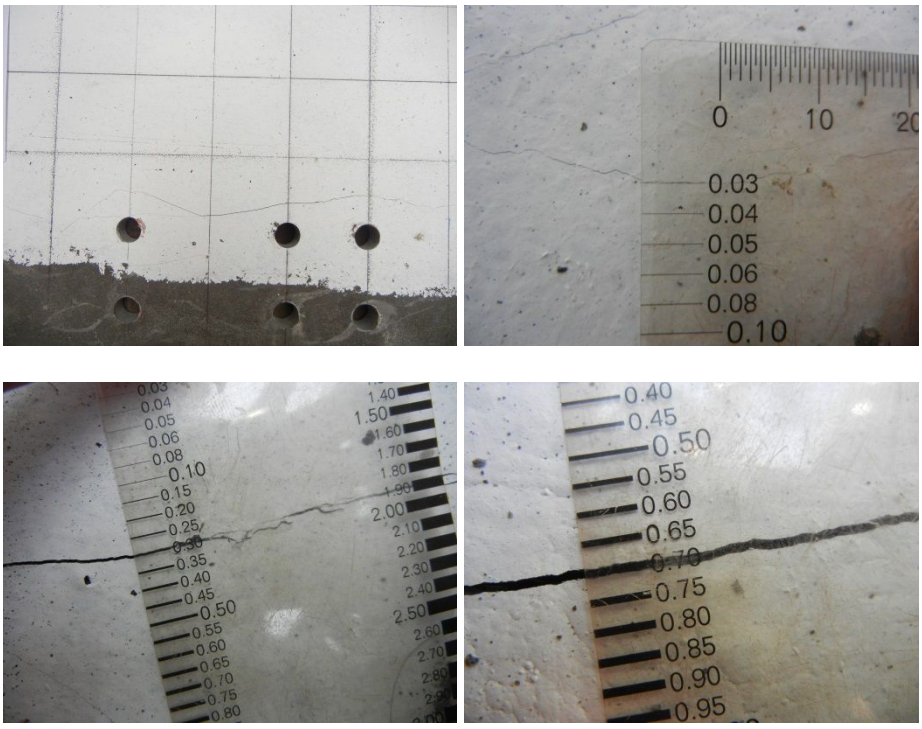

Fig 5-27 Cracking due to the boundary condition

Full restraint of the slab edges was essential for forcing punching

shear failures. Investigation of the slabs after testing showed that the flexural hinges at the support face were not as distinct as the diagonal hinges, indicating that the slabs may not have been fully restrained along the edges. By observing the crack width near the boundary, the crack widths were usually smaller than 0.5mm, but sometimes it has shown little wider crack up to 0.7mm. This could have resulted in a lower load than predicted of a fully restrained slab. From further study, the influence of the boundary condition and the failure behavior should be figured out, and be adopted for the standard.

5.4 Flexural Capacity

The plastic flexural capacity was required to understand the ultimate flexural failure strength. This could be served as the resistance to rotation and deformation of the plastic hinges. As illustrated in **Fig 5-28**, the stress-strain relationship model of UHPC is used as in the previous papers. The UHPC is linear elastic in the compression zone. This linear elastic behavior is continued in the tension region up to the cracking strain, and elastic perfectly plastic when the strain reaches the limiting strain.

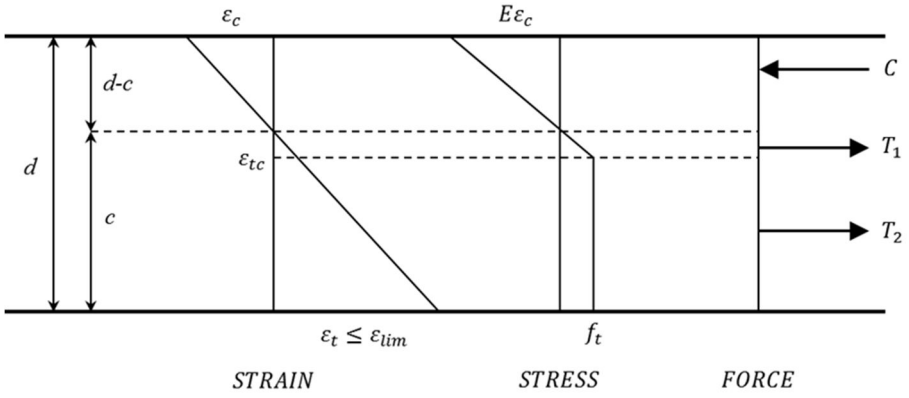

Fig 5-28 Section model for UHPC slab

This stress-strain relationship was used to determine the flexural capacity for various slab thickness. The iterative solution for force equilibrium is used to determine the depth of the compression zone, c. The sectional moment capacity could be calculated by stress distribution from the section model for UHPC slabs of various thickness (**Table 5-2**). The plasticity theory that assumes the square shape of failure section was adopted to determine the ultimate flexural failure strength.

Table 5-2 Sectional Flexural Capacity of UHPC Slabs

	Specimen Name	d [mm]	c [mm]	T_1 [N/m]	T_2 [N/m]	C [N/m]
This Study	D30-f1.5	30	4.80	2.66	285.46	288.12
	D40-f1.5	40	6.40	3.55	380.61	384.16
	D50-f1.5	50	8.00	4.44	475.76	480.2
	D60-f1.5	60	9.60	5.33	570.91	576.24
	D40-f0.0	40	1.06	0.01	63.38	63.39
	D40-f0.5	40	5.07	1.61	302.31	303.92
	D40-f1.0	40	6.11	3.03	363.72	366.75
Joh and et al. (2011)	D40-50-75	40	3.63	0.82	363.72	326.53
	D40-50-100	40	3.63	0.82	363.72	326.53
	D40-50-150	40	3.63	0.82	363.72	326.53
	D70-50-50	70	6.35	1.43	570	571.43
	D70-50-100	70	6.35	1.43	570	571.43
	D70-50-125	70	6.35	1.43	570	571.43

The ultimate flexural failure strength based on the plasticity upper bound solution was calculated as shown in **Table 5-3**. The ultimate punching shear failure strength calculated from the plasticity upper bound solution and the tested failure strength of UHPC slabs were compared to determine the failure mode. The actual failure strength was between the ultimate flexural failure strength and the ultimate punching shear failure strength for most of the UHPC slabs. It could be assumed that the slabs have shown the both failure modes, flexural failure and punching shear failure. Only fiber un-reinforced-40mm-thick-slab shows the smaller flexural failure strength. For the other slabs the ultimate punching shear strength was smaller than the flexural strength. The punching shear failure mode could be determined for the slabs. None

slabs could resist the strength larger than the ultimate flexural failure strength. The failure strength values of the starred slabs were closer to the ultimate flexural failure strength. For the other slabs the tested ultimate strength was closer to the ultimate punching shear strength. It could be assumed that the punching shear governs the failure mode of the other slabs. D40-f0.0 slab is not reinforced by the fibers, so the brittle shear failure could be occurred. However, the ultimate flexural strength was smaller than the ultimate punching shear strength. In this plasticity upper bound solution, the tensile strength of the UHPC was replaced by the term, $0.34\sqrt{f_c}$. This could have the effect on determining the failure mode. For some slabs that have larger loading area were also have larger failure strength. The starred slabs have the ultimate strength close to the ultimate flexural failure strength. It results into the conclusion that the slabs with larger punching area tend to have more flexural failure mode.

Table 5-3 Predicted Ultimate Failure Strength

	Specimen Name	d [mm]	Calculated value		Experimental Value	Failure mode
			$V_{p,flexure}$ [kN]	$V_{p,punching}$ [kN]	V_p [kN]	
This Study	D30-f1.5	30	86.43	28.08	42.185	Punching
	D40-f1.5	40	153.66	42.12	69.05	Punching
	D50-f1.5	50	240.10	58.50	118.94	Punching
	D60-f1.5	60	345.74	77.23	160.795	Punching
	D40-f0.0	40	24.11	42.123	15.43	Flexural
	D40-f0.5	40	119.94	42.123	50.325	Punching
	D40-f1.0	40	146.26	42.123	71.65	Punching
Joh and et al. (2011)	D40-50-75	40	127.10	51.59	78	Punching
	D40-50-100	40	127.10	58.76	106.2	Punching*
	D40-50-150	40	127.10	65.92	91.3	Punching
	D70-50-50	70	389.24	120.38	218.7	Punching
	D70-50-100	70	389.24	145.46	239.5	Punching
	D70-50-125	70	389.24	157.99	296.7	Punching*

5.5 Punching Shear Capacity

The results from the experiment performed by Joh were analyzed with the data from this experiment for feasibility study of the previous equations that were cited in Chapter 2. Same material property was adopted for the experiment performed by Joh so that the K-UHPC code can be used for predicting the punching shear strength. However, the slabs with different fiber reinforcement ratio could not be applied for the code due to the coefficients decided by the material properties. For this paper, the simplified tensile stress vs. crack width graph was assumed by material tests, and adopted on substitution. **Table 5-4** is the outcome from substituting the data.

The ACI code arrangements are highly decentralized ACI does not consider the fiber effects, so the ACI code has small prediction results for UHPC slabs. The experimental data has almost 2.1 times larger value than the predicted results. From this results, the application of ACI code to the UHPC slabs is not reasonable and improvement is essential (**Fig 5-29 (a)**).

Table 5-4 Main Data for Analyzing and the Results

	Specimen Name	ρ_f [%]	d [mm]	f'_c [MPa]	Aspect Ratio	V_{test} [kN]
This Study	D40-f1.5	1.5	40	180	1.0	69.05
	D50-f1.5	1.5	50	180	1.0	118.94
	D60-f1.5	1.5	60	180	1.0	160.80
	D40-f0.0	0.0	40	160	1.0	15.43
	D40-f0.5	0.5	40	160	1.0	50.325
	D40-f1.0	1.0	40	160	1.0	71.65
Joh and et al. (2011)	D40-50-75	2.0	40	180	1.0	78
	D40-50-100	2.0	40	180	1.5	106.2
	D40-50-150	2.0	40	180	2.0	91.3
	D70-50-50	2.0	70	180	1.0	218.7
	D70-50-100	2.0	70	180	2.0	239.5
	D70-50-125	2.0	70	180	2.5	296.7

Narayanan equation calculates the shear strength of concrete, fiber, and reinforcement separately. Narayanan equation is the empirical formula that has coefficients from the material tests. For other material properties the equation could not estimate the strength accurately (**Fig 5-29 (b)**).

As shown in **Fig 5-29 (c)**, JSCE code was the most accurate formula for predicting the punching shear strength. However, JSCE code overestimated the punching shear strength. The results from JSCE were 50% higher than the experimental data. Safety factor for punching shear is needed to be studied by more experiments to get conservative results. JSCE code calculates the matrix and fiber's shear strength individually. The matrix term has reinforcement ratio, so only fiber effects are considered for non-reinforced UHPC slabs like in this paper.

By comparing the code equations with the tested value, the reasonability of the existing formulas could be found. The ratio of the results from existing formula prediction and the tested results was calculated. **Table 5-5** shows the results ratio for having comparison of the code equation in a glance.

UHPC slabs punching shear data was compared with the results from the other code equations. In both the flexural and punching shear failure, the predicted failure loads were higher than the actual failure loads. This trend is understandable for the flexural failures. The interpretation of this difference can likely be attributed to a failure mode different from the predicted failure behavior. From the equations estimation, the slabs with 30mm or 40mm of thickness show higher estimated results than others. It seems that it is because the thin slabs tend to have combined punching shear failure accompanying the flexural failure behavior. The slab is not able to bear the punch load as much as predicted due to the flexural failure behavior.

Table 5-5. Comparison of the Results from Existing Formulas

	Specimen Name	V_{test}[kN]	ACI [kN]	$\frac{V_{test}}{V_{pred.}}$	KCI [kN]	$\frac{V_{test}}{V_{pred.}}$
This study	D40-f1.5	69.05	51.00	1.353	36.87	1.873
	D50-f1.5	118.94	70.84	1.679	51.21	2.323
	D60-f1.5	160.80	93.51	1.720	67.60	2.379
	D40-f0.0	15.43	51.00	0.302	36.87	0.418
	D40-f0.5	50.325	51.00	0.987	36.87	1.365
	D40-f1.0	71.65	51.00	1.405	36.87	1.943
Joh and et al. (2011)	D40-50-75	78	51.00	3.040	41.33	1.887
	D40-50-100	106.2	29.22	3.635	47.05	2.257
	D40-50-150	91.3	32.78	2.785	49.83	1.832
	D70-50-50	218.7	59.87	3.653	96.43	2.268
	D70-50-100	239.5	72.34	3.311	116.52	2.055
	D70-50-125	296.7	78.57	3.776	126.57	2.344

Specimen Name	JSCE [kN]	$\frac{V_{test}}{V_{pred.}}$	Narayanan [kN]	$\frac{V_{test}}{V_{pred.}}$	K-UHPC [kN]	$\frac{V_{test}}{V_{pred.}}$
D40-f1.5	133.99	0.515	57.41	1.203	102.36	0.675
D50-f1.5	186.09	0.639	83.48	1.425	142.17	0.837
D60-f1.5	245.64	0.655	114.24	1.408	187.67	0.857
D40-f0.0	36.07	0.428	74.11	0.208	14.44	1.068
D40-f0.5	56.98	0.883	72.90	0.690	77.58	0.649
D40-f1.0	132.75	0.540	67.33	1.064	96.79	0.740
D40-50-75	115.2	0.677	57.41	1.359	79.83	0.977
D40-50-100	131.2	0.809	62.38	1.702	90.92	1.168
D40-50-150	147.2	0.620	67.36	1.356	102.01	0.895
D70-50-50	268.8	0.814	149.69	1.461	186.28	1.174
D70-50-100	324.8	0.737	167.11	1.433	225.09	1.064
D70-50-125	352.8	0.841	175.82	1.688	244.49	1.214

The experimental data were arranged for comparing the existing formula as illustrated in **Fig 5-29**. From the first graph, the ACI code equation could not estimate the punching shear strength of UHPC properly. The ACI code is for conventional concrete, and does not reflect the effect of the fibers. With larger tested value the code equation tends to underestimate, so the predicted ultimate punching load value is getting less. The application of the code for normal concrete seems inappropriate. For the economical design, the appropriate estimation of strength is necessary that also considered the safety for certain. For this reason, the suitability of the equations that estimate the fiber-reinforced concrete needs to be evaluated.

All the other results of existing formulas represented on the graphs are considering the effect of fibers. The inclinations of the tendency line on all graphs are showing increment. There are not enough test specimens to ensure the reason of increasing tendency. There are two assumptions for it. The first one is that the equations can not properly estimate the ultimate punching strength due to lower amount of fiber reinforcement or excessively thin structure that causes the flexural failure. The second one is that the equations are conservative on reflecting the fiber effect because of the uncertainty on fiber's performance. If the second assumption is the main reason of the increasing tendency, more experiments to confirm the ultimate punching load for the thicker slabs or the slabs made of the higher strength UHPC should be necessary.

The Narayanan equation shows big gap between the slabs with the lower punching load and others. For the other data except for two with lower than 50MPa, the Narayanan's equation underestimates the punching shear strength. The ratio of tested and the predicted punching load was over 1 that represents the conservative design in slab. While the accuracy for the slabs that can resist high strength is good, the supplementation of the equation for the UHPC slab with low fiber volume ratio or the consideration of flexural behavior is essential.

The JSCE code equation shows very even results, but all of the data were located under the line 1. The JSCE code tends to overestimate the punching shear strength of the UHPC slabs. This could not be used in practical estimation, because it does not effectively consider the safety. Also, the inclined trend line seems very suitable except for only a couple of data. For predicting punching shear strength of UHPC slab that was tested in this paper, this equation only considers the fiber's effect. The effect of the matrix is ignored without flexural reinforcement. Even without the consideration of matrix strength, the predicted value was about 50% higher than the experimental value. The supplement for the overestimation will be the burning problem for JSCE code.

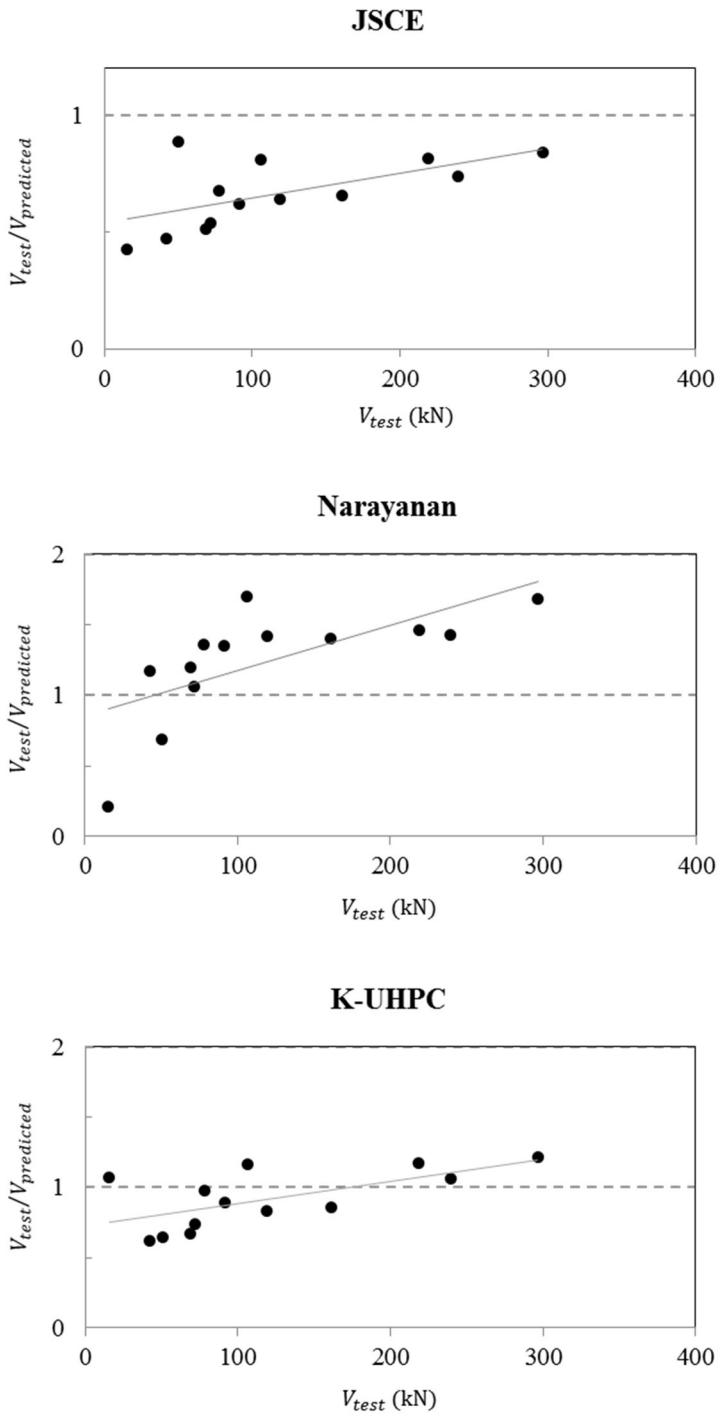

Fig 5-29 Comparison of existing formulas with experimental data

The K-UHPC code equation has the tensile term that considers the relationship between the crack width and the tensile stress from the direct tension test. With the other materials except for the K-UHPC, the crack width - tensile stress curve should be prepared by tests. While there is no specification on tensile strength for all material properties, the application of this equation is hard. The K-UHPC has the advantages that it supplemented the overestimating problem of JSCE and the large distribution problem of Narayanan's equation. However, it shows only little improvements on estimation. The study for the application of material property right into the equation seems to be necessary in further research.

Table 5-6 Distribution for Several Existing Formulas

Equation	Average	Standard Deviation
ACI code	2.22	113%
KCI code	1.90	51.2%
Narayanan	1.24	39.2%
JSCE	0.66	14.2%
K-UHPC	0.92	20.1%

The average and the standard deviation of each code equations are shown in **Table 5-6**. K-UHPC code equation has the closest results with the experimental data. However, K-UHPC code could not be applied for the other experimental data that does not have the K-UHPC material properties, because it is the empirical equation. The constitutive law of UHPC drawn by more tests is to be studied for adoption of material properties.

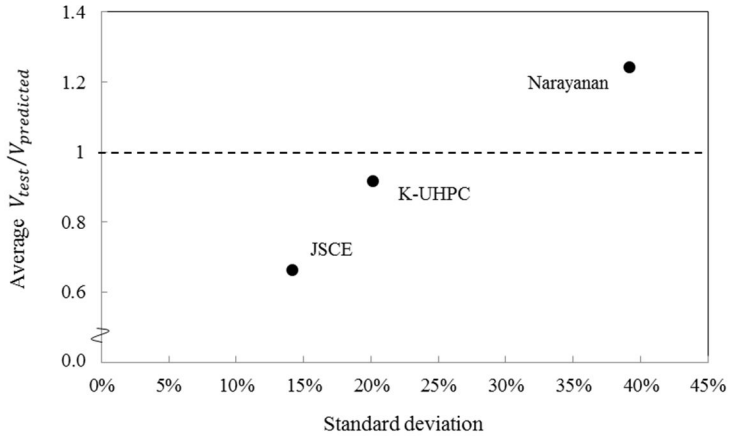

Fig 5-30 Average and Standard Deviation of Ratio of Tested Strength to Predicted Strength by Existing and Code Equations

The formula results except for ACI code result that is not proper for adopting the UHPC model were compared as shown in **Fig 5-30**. Narayanan's equation and JSCE code equation have different disadvantages. The JSCE code is considered as the most suitable equation for UHPC punching shear estimation with the smallest standard deviation, but it has crucial disadvantage that it overestimates the structures. In code equation, the overestimation is very critical problem. When the equation is arranged for designing structures, the most important object is the equation is proper for designing safe structures. Probably, the second one is the economical design. For modifying this problem, the study for proper estimation and the safety factor should be performed. In case of Narayanan's equation, the average of results ratio is little larger than 1, so the safe design will be possible. However, the standard deviation is large. K-UHPC equation supplements these problems. Even though, it shows slightly larger standard deviation than the JSCE code, it predicts the punching shear strength most closely.

Chapter 6. Conclusion

In this paper, the punching shear capacity and the failure behavior of UHPC thin slabs under concentrated load are studied. The data extracted from the research tested punching shear on FRC (fiber-reinforced concrete) slabs were analyzed. In this paper, the UHPC thin slabs were tested for punching shear failure. The experimental results are used for comparing the existing formulas. The following conclusions are based on the tests and analysis:

- Narayanan's equation calculates the shear strength of matrix, flexural reinforcement, and fibers individually. It has the disadvantage of empirical formula that the coefficients for each term are from experiments. It is hard to be applied for structures with other material properties.

- The tensile behavior of UHPC was examined. The crack width does not show the relationship according to the fiber volume ratio. The proof of change in the crack width according to the other fiber's properties such as the fiber's length, diameter, and shape should be done.

- The tensile strength of 1.0% and 1.5% fiber-reinforced UHPC does not have big gap, and the 1.0% UHPC shows more even results. It is considered due to the fiber's directivity. From this result, the usage of 1.0% UHPC is better for confirming the strength and for economic.

- The thicker slab could resist to higher punching strength, and the ultimate punching shear strength was inversely proportional to the deflection.

- The punching shear strength and deformation were proportionally increased as fiber volume ratio increased. The behavior of 1.0% and 1.5% fiber-reinforced UHPC slabs was almost same.

- The tensile strength from the direct tension test and the punching shear strength was not in proportional relationship. The un-unified crack width and the fibers directivity that is difficult to control are assumed for the reason. The average tensile strength according to the crack width seems the most proportional to the punching load.

- The critical part could be determined in the strain distribution graph. The slab with flexural failure behavior has the largest strain near the boundary, while the slab that mainly shows punching shear failure behavior has the largest strain near the punching area.

- The initial inclinations of the strain response according to the fiber volume rate do not show big difference. When it goes to the maximum strain, the slabs with more fiber reinforcement have increased inclination.

- Except for 30mm-thick slab, the total inclination of strain was getting higher with the increment of thickness, but the deformation capacity was almost same. Thicker slabs tend to be failed in brittle manner. It was concerned that the 30mm-thick slab did not follow this assumption because of its flexural behavior.

- While the conventional concrete slabs tend to have the failure section three to four times of depth far from the loading pad, UHPC flat plate punching crack was occurred five to six times of depth far from the loading pad. It is assumed that the UHPC slab has gentle strut angle smaller than $45°$.

- For punching shear failure, the flexural behavior that reduces the resistance to the punching load was shown on thin slabs. The punching shear strength equation overestimated for the thin slabs. In further study, the minimum slab thickness can be proposed.

- Fibers allow the slabs to have the ductile failure. However, as the thickness of the slab is increasing, the slab has higher punching shear strength and more brittle failure.

- The deflection-punching load curve shows uneven line due to the fiber effects. While the fibers control the micro-crack, the load increases. As the fibers failed, the load slightly decreases with small noise.

- JSCE code, Narayanan, and K-UHPC code equations were analyzed for confirming its feasibility.

    - In this paper, JSCE shows the least standard deviation, but it overestimates the punching shear strength. For safety reason, JSCE should be revised in further study.

    - K-UHPC code has the closest results to the experimental value. However, the relationship of crack width and tensile strength is hard to be applied without extra experiments. For developing this equation, the study for finding the constitutive law or the method applying material properties directly can be performed in further study.

    - Narayanan equation is the only one formula that has the fiber volume ratio term directly. However, it shows larger standard deviation than the others. The main cause of large standard deviation is considered due to the empirical coefficients. The relationship between the material property and the strength should be defined.

- The absence of the constitutive law of the UHPC was the most crucial part on estimating UHPC slabs' punching shear strength. The experiments to find out the relationship between the deformation and strength according to the material property should be performed in further study.

References

A. M. Shaaban and H.Gesund, “Punching Shear Strength of Steel Fiber Reinforced Concrete Flat Plates”, ACI Structural Journal, 1994, Title no. 91-S40, pp.406-414

ACI 318M-08, “Building Code Requirements for Structural Concrete and Commentary, ACI Committee 318, 2008, pp.430

AFGC, “Ultra High Performance Fiber-Reinforced Concrete Recommendations”, AFGC, 2013, pp.358

Aurelio Muttoni, “Punching Shear Strength of Reinforced Concrete Slabs without Transverse Reinforcement”, ACI Structural Journal, 2008, Title no.105-D42, pp.440-450

Aurelio Muttoni and Schwartz, J., “Behavior of Beams and Punching in Slabs without Shear Reinforcement”, IABSE Colloquium, 1991, pp.703-708

Devin K. Harris, “Characterization of Punching Shear Capacity of Thin UHPC Plates”, Master’s Thesis, Blacksburg, Virginia, 2004,131pp.

F. R. Miguel and et al, “Applications of Critical Shear Crack Theory of Reinforced Concrete Slabs with Transverse Reinforcement”, ACI Structural Journal, 2009, Title no. 106-S46, pp.485-494

Hiroshi Higashiyama and et al, “Design Equation for Punching Shear Capacity of SFRC Slabs”, *International Journal of Concrete Structures and Materials*, 2011, Vol 5, No.1 pp.35-42

Joh, Chang Bin and et al, “UHPC 바닥판 슬래브의 뚫림전단강도”, 구조물진단학회지, 2011

JSCE, “Recommendations for Design and Construction of High Performance Fiber Reinforced Cement Composites with Multiple Fine Cracks (UHPCC)”, Concrete Engineering Series, 2007

KCI, “Design Guidelines for Ultra High Performance Concrete K-UHPC Structure”, Korea Concrete Institute, 2012

Kiang-Hwee Tan and P.Paramasivam, “Punching Shear Strength of Steel Fiber Reinforced Concrete Slabs”, J. Master Civil Engineering, 1994, pp.240-253

L. F. Maya and et al, “Punching Shear Strength of Steel Fibre Reinforced Concrete Slabs”, Engineering Structures 40, 2012, pp.83-94

R. N. Swamy, “Punching Shear Behavior of Reinforced Slab-Column Connections Made with Steel Fibers Concrete”, *ACI Journal*, 1984, Title no. 79-41, pp.392-406

R. Narayanan and I.Y.S. Darwith, “Punching Shear Tests on Steel-Fiber-reinforced Micro-concrete Slabs”, Magazine of Concrete Research, 1987, Vol.39, No138, pp.42-50

RILEM, “Designing and Building with UHPC: from innovation to large-scale realizations”, 2013, pp.810

Stefano Guandalini and et al, “Punching Tests of Slabs with Low Reinforcement Ratios”, ACI Structural Journal, 2009, Title no.106-S10, pp.87-95

초 록

UHPC 슬래브의 뚫림전단강도 산정 및 파괴거동 연구

박지현

건축학과 건축구조전공

서울대학교 대학원

최근 고강도, 고연성 및 고내구성의 장점이 있는 UHPC에 대한 연구가 활발히 진행되고 있다. UHPC에 보강된 강섬유가 인장 균열을 억제하기 때문에 기존 콘크리트보다 인장력이 크고, 인장력에 영향을 많이 받는 뚫림전단력 향상에 기여할 것으로 여겨진다. 하지만 UHPC의 구조 성능을 확실히 정의하고 구조 설계에 적용할 수 있는 위한 연구가 필요하다. 따라서 기존 산정식의 적합성을 판단하고 파괴 형상을 관찰하는 것이 이번 연구의 목적이다.

선행연구에서는 강섬유 효과에 대한 이해를 위해 강섬유 보강 콘크리트 슬래브 실험 자료를 수집하여 분석하였다. 강섬유, 콘크리트와 휨보강 철근의 영향을 각각 구하여 합산하는 방식의 Narayanan이 제시한 식이 가장 적합한 것으로

보여졌다. 하지만 각 항의 계수들이 실험 데이터에 의한 값으로 다른 재료 특성에 대해서 오차가 크게 나타난다는 단점이 있었다.

이번 연구에서는 슬래브 두께와 강섬유 부피비가 다른 총 7개의 UHPC 슬래브를 실험하였으며, 재료특성의 확인을 위해 강섬유 부피비가 다른 UHPC에 대해서 인장실험도 진행하였다. 강섬유 부피비가 증가하며 최대 인장 응력은 증가했지만, 균열폭은 큰 차이가 없었다. 1%와 1.5% 강섬유 보강 UHPC는 인장실험과 뚫림전단 실험에서 모두 큰 차이가 없는 것으로 나타났다. 하지만 1% UHPC의 실험체 결과값은 편차가 크지 않은 반면, 1.5% 실험체의 결과값은 편차가 매우 크게 나타나 강도 확보나 경제성을 위해 1% 보강이 적절할 수 있음을 확인하였다.

K-UHPC에서 제안한 균열폭을 고려한 설계평균인장강도가 뚫림전단강도에 비례하는 형태를 보여, 설계평균인장강도의 적용이 강섬유 부피비를 적용함에 있어 유리함을 확인하였다. 하지만, 최대인장응력은 뚫림전단강도에 비례하지 않은 형태를 보였다. 이는 슬래브의 균열폭이 일정하지 않으며, 작은 인장시험체에 비해 강섬유의 방향성을 조절하기 어렵기 때문인 것으로 보여진다.

기존 콘크리트는 균열이 재하면에서 슬래브 두께의 2~3배 떨어진 지점에서 주로 발생하는데 비해 UHPC 슬래브는 4~5배 먼 곳에서 발생한다. 또한 기존 콘크리트 파괴면에 비해

잔균열이 많이 발생한 것으로 보아 강섬유 효과가 작용했음을 확인할 수 있었다.

얇은 두께인 30m와 40mm 슬래브는 뚫림전단 산정식이 과대평가하는 경향을 보였다. 변형율 곡선과 파괴 단면을 확인한 결과 휨파괴의 영향을 받아 뚫림전단에 대한 저항성이 떨어진 것으로 확인할 수 있었다.

실험 결과값을 분석하여 기존 뚫림전단 산정식의 타당성을 파악하고자 하였다. JSCE 식은 가장 작은 편차를 보여주었지만, 약 50% 정도 과대평가하는 경향을 보였다. 안전성과 사용성을 위해 이에 대한 보완이 필요할 것으로 보인다. K-UHPC 식은 실험값과 가장 근사한 값을 예측하였다. 하지만 JSCE에 비해 편차가 크게 나타나고, 재료 특성을 반영하지 못해 이에 대한 추가 연구가 필요할 것으로 보인다.

Keywords : Failure model; Punching shear strength; UHPC
Student Number : 2013-20560